





Extent of alteration, paleomagnetic history, and infrared spectral properties of the Tarda ungrouped carbonaceous chondrite

H. C. BATES ^{1,*}, R. ASPIN², C. Y. FU³, C. S. HARRISON^{1,4}, E. FEAVER⁵,
E. BRANAGAN-HARRIS^{1,6}, A. J. KING ^{1,*}, J. F. J. BRYSON ², S. SRIDHAR ², and
C. I. O. NICHOLS²

¹Planetary Materials Group, Natural History Museum, London, UK

²Department of Earth Sciences, University of Oxford, Oxford, UK

³Department of Earth Science & Engineering, Imperial College London, London, UK

⁴Department of Earth & Environmental Sciences, The University of Manchester, Manchester, UK

⁵Physics & Astronomy Department, University College London, London, UK

⁶Atmospheric, Oceanic & Planetary Physics, University of Oxford, Oxford, UK

*Correspondence

H. C. Bates and A. J. King, Planetary Materials Group, Natural History Museum, London, UK.

Email: h.bates@nhm.ac.uk and a.king@nhm.ac.uk

(Received 12 April 2024; revision accepted 28 May 2024)

Abstract–Tarda is an ungrouped, hydrated carbonaceous chondrite (C2-ung) that was seen to fall in Morocco in 2020. Early studies showed that Tarda chemically resembles another ungrouped chondrite, Tagish Lake (C2-ung), which has previously been linked to the dark D-type asteroids. Samples of D-type asteroids provide an important opportunity to investigate primitive conditions in the outer solar system. We show that Tarda contains few intact chondrules and refractory inclusions and that its composition is dominated by secondary Mg-rich phyllosilicates (>70 vol%), carbonates, oxides, and Fe-sulfides that formed during extensive water–rock reactions. Quantitative assessment of first-order reversal curve (FORC) diagrams shows that Tarda’s magnetic mineralogy (i.e., framboidal magnetite) is comparable to that of the CI chondrites and differs notably from that of most CM chondrites. These traits support a common formation process for magnetite in Tarda and the CI chondrites. Furthermore, Tarda’s pre-terrestrial paleomagnetic remanence is similar to that of Tagish Lake and samples returned from asteroid Ryugu, with a very weak paleointensity (<0.6 μ T) suggesting that Tarda’s parent body accreted more distally than that of the CM chondrites, possibly at a distance of >5.4–8.3 AU. An origin in the cold, outer regions of the solar system is further supported by the presence of distinct, porous clasts enriched in aliphatic-rich organics that potentially retain a pristine interstellar composition. Together, our observations support a genetic relationship between Tarda and Tagish Lake.

INTRODUCTION

Carbonaceous chondrite meteorites offer unique insights into processes that occurred in the early solar system. The hydrated CM (Mighei-type) and CI (Ivuna-type) chondrites likely originate from C-complex asteroids; dark, volatile-rich bodies that are hypothesized to have contributed to the delivery of water and prebiotic

organic molecules to the terrestrial planet-forming region (e.g., Alexander et al., 2012; King et al., 2022; Morbidelli et al., 2000; Vacher et al., 2020). However, there are an increasing number of ungrouped carbonaceous chondrites in our meteorite collections, some of which show similarities to the CM and CI groups but also display enough key differences to have likely formed in distinct regions of the protoplanetary disk.

One such meteorite is Tarda, an ungrouped type 2 carbonaceous chondrite (C2-ung), which was seen to fall in southern Morocco on August 25, 2020. A total of ~4 kg of material were recovered within days of the fall, with many stones found using magnets. Initial petrographic observations showed that Tarda is a breccia, with small chondrules, chondrule fragments, and amoeboid olivine aggregates (AOAs) embedded within a fine-grained matrix (~80 vol%) of phyllosilicates (serpentine and smectite), magnetite, sulfides (pyrrhotite, pentlandite, troilite), carbonates (dolomite, siderite), and anhydrous silicates (olivine, pyroxene) (Chennaoui Aoudjehane et al., 2021; Gattacceca et al., 2021). Tarda has a bulk oxygen isotopic composition that lies between the CI and CY (Yamato-type) chondrites, although its $\Delta^{17}\text{O}$ value is lower than both, plotting below the terrestrial fractionation line (TFL) (Chennaoui Aoudjehane et al., 2021). In fact, its bulk oxygen isotopic composition is most similar to another C2-ung chondrite, Tagish Lake, which fell in Canada in 2000 (Brown et al., 2000). A link between Tarda and Tagish Lake is also supported by their bulk elemental compositions, high C/H ratios, comparable enrichments in deuterium, ^{13}C , and ^{15}N (Marrocchi et al., 2021) and noble gas signatures (Avicé et al., 2022).

The Tagish Lake meteorite has been extensively studied since its fall, with many of its petrographic (e.g., hydrated mineralogy, relatively few chondrules, or calcium-aluminum-rich inclusions (CAIs)) and geochemical properties (e.g., high carbon content, ^{13}C -rich carbonates) pointing toward an origin in the cold, outer regions of the solar system (Brown et al., 2000; Fujiya et al., 2019; Zolensky et al., 2002). Tagish Lake is also extremely friable, has a particularly low density (Zolensky et al., 2002), and recorded a very weak ancient magnetic field that is consistent with the formation of its parent body at >8–13 AU (Bryson, Weiss, Lima, et al., 2020). Based on its reflectance spectrum, Hiroi et al. (2001) proposed that Tagish Lake could represent a sample of the carbon-rich D-type asteroids, which are generally found in the outer main asteroid belt and Jupiter's Trojan population (e.g., DeMeo & Carry, 2014; Dotto et al., 2006). However, D-type asteroids may have formed as far out as the Kuiper Belt before being scattered inward to their present-day locations during orbital instabilities and migration of the giant planets (e.g., Levison et al., 2009; Morbidelli et al., 2005). As such, D-type asteroids are likely key witnesses to materials and conditions during the early history of solar system formation.

Here, we describe the mineralogy and petrography, bulk water contents, and paleomagnetic characteristics of the Tarda C2-ung chondrite. We show that Tarda shares a genetic relationship to Tagish Lake and records extensive water-rock reactions on a parent body that accreted in the outer regions (>5 AU) of the solar system. In addition, we

present infrared (IR) spectra of Tarda acquired at the bulk and microscale that further constrain the nature of alteration and offer a ground truth for remote asteroid observations, including NASA's Lucy mission to characterize the composition of Jupiter's Trojans, and JAXA's Martian Moons eXploration (MMX) mission to Phobos, which has spectral features similar to the D-type asteroids.

METHODS

X-Ray Diffraction

An approximately 200 mg fusion crust free chip of Tarda was powdered and homogenized using an agate mortar and pestle. A small aliquot of the powder was placed into a 0.9 mm quartz glass capillary and then loaded into a STOE STADI MP X-ray diffractometer (XRD) equipped with a Mythen2 2K double detector system at the Natural History Museum (NHM), London. An initial powder diffraction pattern was acquired from ~4° to 77° (2 θ) with a time/step of 1800 s using Mo K α radiation. The sample was rotated continuously throughout the measurement and mineral phases were identified using the International Centre for Diffraction Data (ICDD) database (PDF-2).

The bulk mineralogy of Tarda was determined using position sensitive detector (PSD-) XRD at the NHM, London. Approximately 50 mg of the powder was loaded into an aluminum sample well and analyzed using an Enraf-Nonius PDS120 XRD with an INEL curved 120° PSD. The detector remained in a static geometry relative to the primary X-ray beam (Cu K α_1) and sample stage, the latter of which was rotated continuously throughout each measurement. X-ray diffraction patterns were collected from Tarda for 16 h and from mineral standards prepared in the same way for 30 min. Silicon and silver behenate were used to calibrate the instrument and the intensity of the primary beam was monitored by measuring a polished Fe-metal block at regular intervals during the experimental session. Mineral abundances were quantified using a profile-stripping method, with detection limits of ~1 vol% and uncertainties on the order of ~2 vol% (e.g., Bland et al., 2004; Cressey & Schofield, 1996; Howard et al., 2009; King, Schofield, et al., 2015).

Scanning Electron Microscopy

Two small chips (~3–4 mm in size) of Tarda were set in epoxy resin and polished using ethylene glycol (ethane-1,2-diol) and aluminum oxide in the mineral preparation laboratory at the NHM, London. The mineralogy and petrography of the polished samples were qualitatively characterized using a ZEISS EVO 15LS scanning electron

microscope (SEM) with an Oxford Instruments AZtec energy-dispersive X-ray (EDS) system and 80 mm² X-Max silicon drift detector (SDD) at the NHM, London. Full-section backscattered electron (BSE), secondary electron (SE), and EDS element maps were acquired at an accelerating voltage of 20 kV and a beam current of 1.5 nA. EDS data were processed and analyzed using the Oxford Instruments Aztec software. ImageJ was used to layer the overview maps and determine the area% of mineral phases, with grains that were <10 pixel units in size (corresponding to a grain size of <5 µm) discounted from the calculation. Additional BSE/SE images and EDS maps of regions/assemblages of interest were collected using an FEI Quanta 650 field-emission SEM equipped with a Bruker Quantax EDS system and FlatQUAD SDD at 9 kV.

Thermogravimetric Analysis

The abundance of water in Tarda was estimated by heating ~12 mg of the homogenized powder using a TA Instruments Simultaneous Thermal Analysis SDT Q600 thermogravimetric analyzer (TGA) at the NHM, London. This measurement was conducted in December 2020, approximately 4 months after the fall. The powder was loaded into an alumina crucible and placed onto the TGA balance. Mass loss was then recorded as the sample was heated in a sealed furnace from room temperature (~20–25°C) to 1000°C at a rate of 10°C min⁻¹ under an N₂ flow of 100 mL min⁻¹. The abundance of water was calculated by assuming that all mass loss from 200 to 770°C resulted from dehydration and dehydroxylation of –OH/H₂O-bearing minerals, although this is known to be an overestimate as other phases, such as sulfides, carbonates, and organics, will also breakdown and contribute to mass loss in this temperature range (Bates et al., 2023; Garenne et al., 2014; King, Solomon, et al., 2015).

FORC Diagrams

The properties (e.g., size, proximity, morphology, arrangement) of Tarda's magnetic grains were investigated by measuring first-order reversal curve (FORC) diagrams of two subsamples (<1 mg) of the homogenized powder. To construct these diagrams, we measured and processed FORCs using the procedures outlined in Sridhar et al. (2021) (see the [Supplementary Materials](#) for details). The FORCs were measured using the MicroMag 2900 Series alternating gradient magnetometer (AGM) at the University of Cambridge. Based on the XRD and SEM data, as well as FORC diagrams and paleomagnetic studies of CM chondrites (Cournède et al., 2015; Sridhar et al., 2021) and Tagish Lake (Bryson, Weiss, Lima, et al.,

2020), we expect the predominant magnetic mineral in Tarda's FORC diagram to be magnetite.

Paleomagnetism

Most pieces of Tarda were collected from the field using artificial magnets, increasing the likelihood that Tarda's pre-terrestrial paleomagnetic remanence will be challenging to access and interpret due to overprints. We tested several pieces of Tarda (using a handheld fluxgate magnetometer) and found that an aliquot of the material used in this study displayed the weakest magnetization, suggesting that it carries the smallest overprints. As such, it is the most likely sample of Tarda to yield its pre-terrestrial remanence. Paleomagnetic analysis was therefore performed on small particles (named 2a–2d, and ~2 to 4 mm in size) taken from this sample. The unconsolidated and unoriented nature of these particles means that we were unable to recover their mutual remanence directions. Furthermore, none of the material in this aliquot carried fusion crust, so we are unable to determine the original distance of these pieces from the fusion crust.

We measured the natural remanent magnetization (NRM) carried by each of these Tarda specimens using a 2G Enterprises Superconducting Rock Magnetometer model 755R housed in the magnetically shielded room at the University of Oxford. We then removed the NRM carried by each specimen using alternating field (AF) demagnetization, measuring the NRM remaining throughout this process. To constrain the ancient field intensity experienced by Tarda, we then applied several anhysteretic remanent magnetizations (ARMs) with a constant peak AF intensity (200 mT) and a range of bias field values (1, 10, and 100 µT) using an ASC Scientific D-2000 AF Demagnetizer, which we subsequently AF demagnetized using the same procedure as the NRM. We chose to adopt AF demagnetization methods rather than thermal methods due to the pronounced alteration observed on heating of Tagish Lake to even low temperatures (Bryson, Weiss, Lima, et al., 2020), suggesting that Tarda would also very likely yield unreliable thermal demagnetizations. For full details of the paleomagnetic analysis, see the [Supplementary Materials](#).

Infrared Spectroscopy

Near (NIR) and mid-infrared (MIR) diffuse reflectance spectra between 1.7 and 50 µm (6000–200 cm⁻¹) were collected from an ~50 mg aliquot of the homogenized Tarda powder using a Bruker VERTEX 70v Fourier Transform Infrared Spectrometer at the Planetary Spectroscopy Facility at the University of Oxford. All measurements were obtained under vacuum

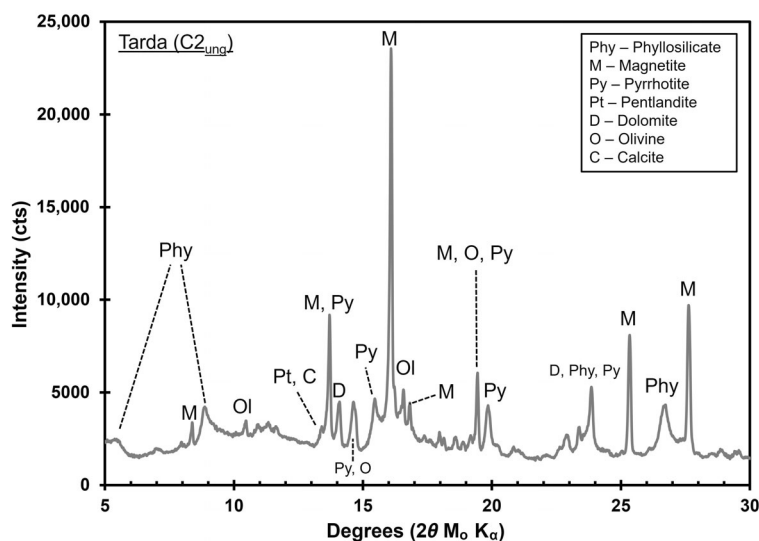


FIGURE 1. XRD pattern of Tarda collected using an STOE STADI MP X-ray diffractometer at the NHM, London. The main minerals identified include phyllosilicates (Phy), magnetite (M), pyrrhotite (Py), pentlandite (Pt), dolomite (D), olivine (Ol), and calcite (C).

(~2 hPa) at a spectral resolution of 4 cm^{-1} , and the final spectra are an average of 250 scans. A wide range mid- to far-IR (MIR-FIR) beam splitter and a room temperature deuterated L-alanine doped triglycine sulfate (RT-DLaTGS) detector were used; instrumental effects were removed by dividing the sample spectrum by that of a diffuse gold calibration target. The positions of features of interest were determined using spectral analysis procedures previously described by Donaldson Hanna et al. (2012) and Bates et al. (2020, 2021, 2023) (see the [Supplementary Materials](#) for details).

The spectral properties of the polished Tarda samples were determined using a Thermo Nicolet iN10 infrared imaging microscope with a liquid-N₂ cooled mercury cadmium telluride (MCT) detector at the NHM, London. Reflectance spectral maps were collected from 2.5 to $18\text{ }\mu\text{m}$ ($4000\text{--}500\text{ cm}^{-1}$) with a spectral resolution of 4 cm^{-1} . The spot size of the IR beam was restricted to $75 \times 75\text{ }\mu\text{m}$ and the maps were set up with step sizes of $75\text{ }\mu\text{m}$ (Figure S1). Each spectrum is the average of 64 scans and the background was corrected using the spectrum of a polished gold sample that was measured every 30 min during the experimental session.

We note that the polished Tarda surface was not completely flat, with the topography appearing to influence the spectra acquired from some areas (see the [Supplementary Materials](#) for details, Figure S2). The positions of spectral features, therefore, were only determined for spectra from selected regions of the sample. In addition to positions, we also calculated the depth of the 3.4 and $6\text{ }\mu\text{m}$ features, respectively, to evaluate variations across the regions of interest. For this, we

normalized the spectrum to a linear continuum fit to points on either side of the feature and calculated the difference between the minimum reflectance of the feature and the reflectance at the continuum.

RESULTS

Mineralogy and Petrography

The main crystalline phases identified in Tarda by XRD are olivine, magnetite, carbonate (dolomite), and Fe-sulfide (pyrrhotite) (Figure 1). Broad features at $\sim 5.4^\circ$, $\sim 8.9^\circ$, and $\sim 26.7^\circ$ ($2\theta\text{ Mo K}\alpha$) are attributed to fine-grained, poorly crystalline Mg-rich phyllosilicates (serpentine and smectite). The XRD pattern of Tarda is similar to those of the CI chondrites; it lacks the peaks from relatively crystalline Fe-bearing serpentine that are typically seen for CM chondrites (e.g., Howard et al., 2009; King, Schofield, et al., 2015).

Phyllosilicates are the most abundant (~72 vol%) phase in Tarda, followed by olivine (~10 vol%), magnetite and Fe-sulfide (both ~8 vol%), and carbonate (~2 vol%) (Table S1). Tarda has a phyllosilicate fraction ($\text{PSF} = \text{total phyllosilicate abundance} / [\text{total anhydrous silicate} + \text{total phyllosilicate abundance}]$) of 0.88, which corresponds to a petrologic subtype of 1.3 on the scale of Howard et al. (2015).

The bulk XRD results are supported by the petrographic observations of polished Tarda samples. Figure 2 shows a BSE image and Ca-Mg-Fe EDS map of Tarda; the most abundant phase is a fine-grained Mg- and Fe-bearing phyllosilicate matrix in which grains and

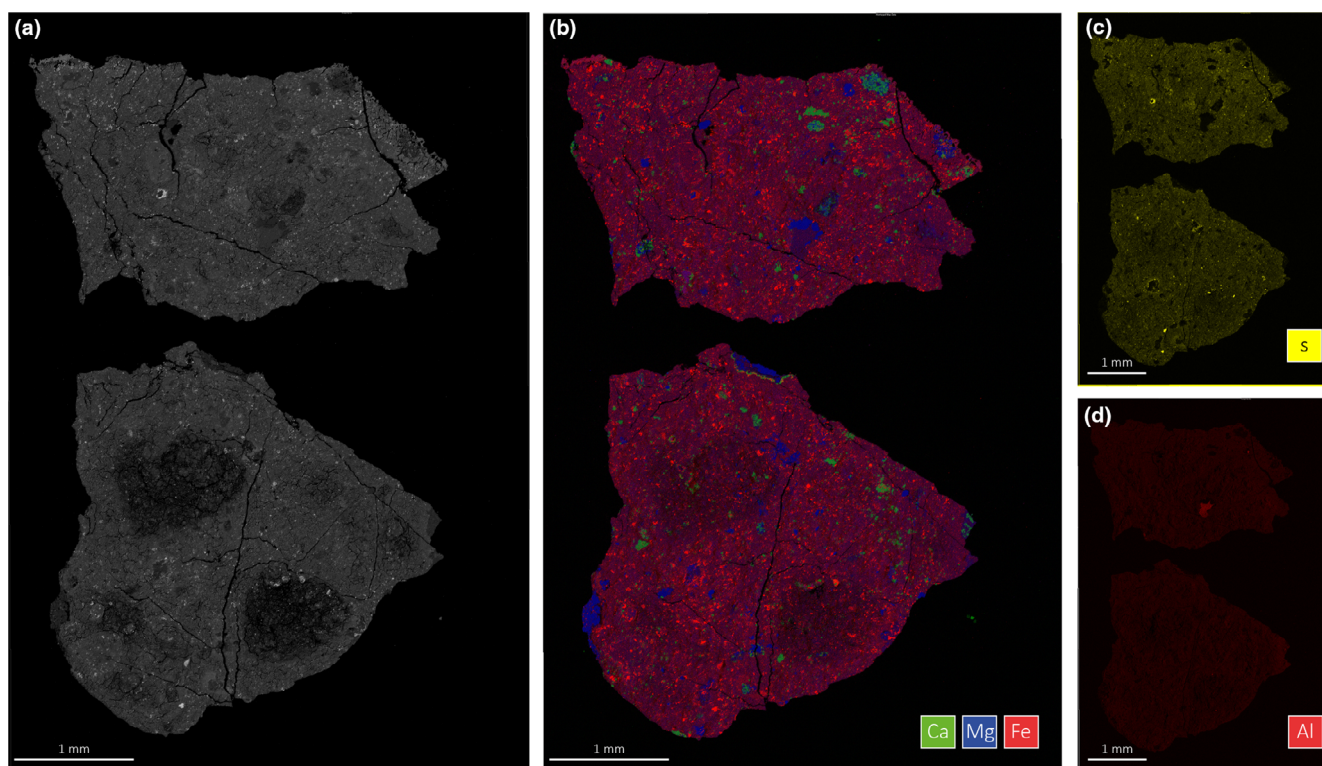


FIGURE 2. (a) Overview of BSE images and EDS maps showing (b) combined calcium (green), magnesium (blue), and iron (red); (c) sulfur; and (d) aluminum in two polished Tarda samples.

clusters of magnetite, dolomite, and Fe-sulfides are embedded. No intact chondrules or CAIs were identified, but chondrule fragments and other silicate grains (Figure 3a), including the remnants of an Al-rich chondrule glass (Figure 2d), and possible chondrule pseudomorphs are present.

Magnetite is typically framboidal in morphology and found as clusters of either small ($<1\ \mu\text{m}$) grains or larger ($>1\ \mu\text{m}$) individual grains in the matrix (Figure 3b), with coarse grains ($>5\ \mu\text{m}$) comprising 3.3 ± 1.1 area% of the polished samples. In one instance, magnetite framboids pseudomorph what was likely an Fe-sulfide lath (Figure 3c), while magnetite is also found as rims around coarse phyllosilicates or partially altered anhydrous silicates (Figure 3d). Carbonates are predominantly dolomite and $<50\ \mu\text{m}$ in size, although the largest carbonate grains are up to $\sim 100\ \mu\text{m}$ (Figure 3e). Iron sulfides ($>5\ \mu\text{m}$) comprise 0.2 ± 0.1 area% of the polished samples and are mainly pyrrhotite, with a few Ni-bearing pentlandite grains also observed. The largest pyrrhotite grains often have a porous or “spongy” texture (Figure 3f).

Abundance of Water

Figure 4 shows the mass loss and derivative of mass loss (DTG) curves for Tarda and the CI chondrite

Orgueil. The TGA curves are divided into distinct temperature ranges based on the expected breakdown and decomposition of different minerals: mass loss at $<200^\circ\text{C}$ is attributed to the removal of adsorbed terrestrial water and breakdown of sulfates; from 200 to 400°C and $400\text{--}770^\circ\text{C}$ due to the release of $-\text{OH}/\text{H}_2\text{O}$ in Fe-(oxy)hydroxides and phyllosilicates, respectively; and between 770 and 900°C from CO_2 produced during the breakdown of carbonates (Table S2; Garenne et al., 2014; King, Solomon, et al., 2015). Assuming all mass loss between 200 and 770°C is due to the dehydration and dehydroxylation of phyllosilicates, we estimate that the abundance of water in Tarda is $\sim 12.5\ \text{wt}\%$.

Magnetic Mineralogy

FORC diagrams from two subsamples of the Tarda powder are very similar, consisting of a distinctive triangular background behind a peak at a coercivity of 10–15 mT and a slightly negative interaction field value (Figure 5). These traits are almost identical to the FORC diagram of Tagish Lake (Bryson, Weiss, Lima, et al., 2020) and Wisconsin Range (WIS) 91600 (CM-an) (Bryson, Weiss, Biersteker, et al., 2020), and resemble those of the CI chondrites (Sridhar et al., 2021) and Ryugu (Sato et al., 2022).

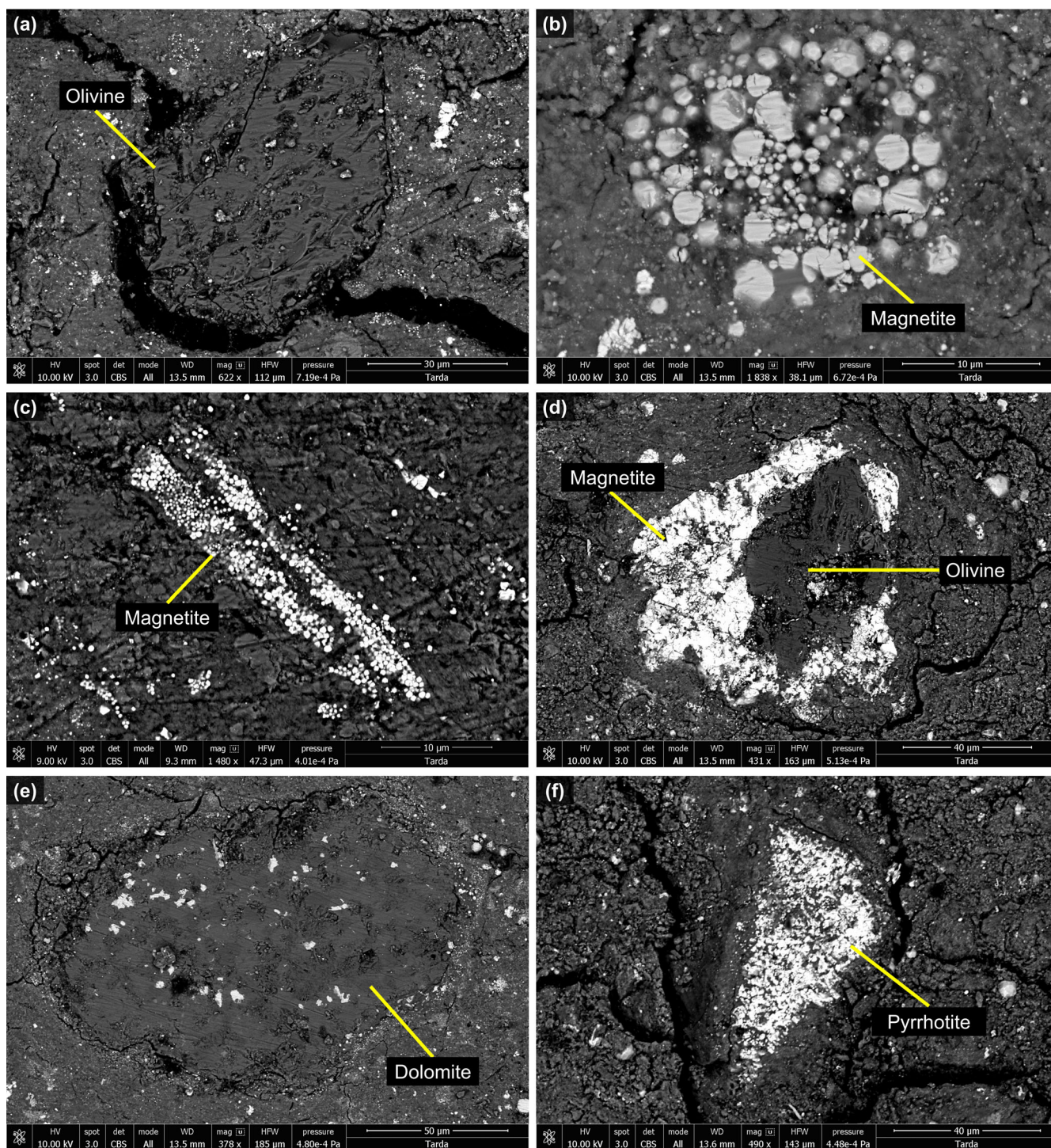


FIGURE 3. BSE electron images showing examples of (a) a partially altered olivine grain, (b) a cluster of magnetite grains, (c) magnetite pseudomorph of an Fe-sulfide grain, (d) magnetite rim around an olivine grain, (e) a large dolomite grain, and (f) a pyrrhotite grain in the Tarda meteorite.

The similarity between FORC diagrams from different meteorites (WIS 91600, CI chondrites, and CM1.0–1.2 chondrites) has been quantified previously using principal component analysis (PCA) (Sridhar et al.,

2021). The existing FORC diagram of Tagish Lake (Bryson, Weiss, Lima, et al., 2020) was measured using different parameters and, therefore, cannot be included in this analysis. We included the FORC diagrams from

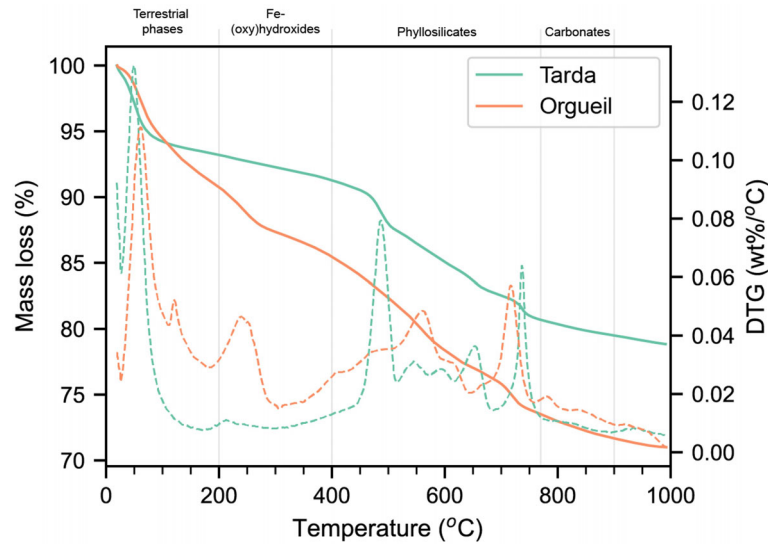


FIGURE 4. Mass loss and DTG curves for Tarda and the CI chondrite Orgueil (data from King, Solomon, et al., 2015). Mass loss events are attributed to terrestrial water and sulfates (<200°C), the release of $\text{-OH/H}_2\text{O}$ from Fe-(oxy)hydroxides (200–400°C) and phyllosilicates (400–770°C), and CO_2 from the breakdown of carbonates (770–900°C). Mass loss between 200 and 770°C was used to estimate the abundance of water in Tarda.

Tarda into this analysis, finding that the principal component scores of Tarda and the CI chondrites are very similar (Figure 5c). This result indicates that these meteorites share almost identical magnetic mineralogies (i.e., sizes, proximities, morphologies, and arrangements of magnetite grains). This is consistent with petrographic observations showing that both Tarda (Figure 3) and the CI chondrites (e.g., Alfing et al., 2019) contain abundant magnetite framboids and plaquettes.

Paleomagnetism

Table S3 summarizes the AF demagnetization of the NRM of Tarda specimens 2a–2d, and Figure 6 shows the corresponding orthogonal projection diagrams. Each specimen carries low coercivity (0 to 6–16 mT depending on the specimen; LC) and medium coercivity (6–16 mT depending on the specimen; MC) components that display much larger magnetic moments than equivalent components carried by most other CM and C2-ung chondrites (Bryson et al., 2023; Bryson, Weiss, Biersteker, et al., 2020; Bryson, Weiss, Lima, et al., 2020; Cournède et al., 2015). Due to the unconsolidated nature of the parent powder (see Methods section), we are unable to determine if these components are mutually orientated among the specimens. However, the LC and MC components are within $\sim 20^\circ$ – 40° of each other for the same specimen, suggesting a similar origin for these components. The LC and MC components also show comparatively small mean angular deviation (MAD) values of 1.8° – 12° for the LC component and 2.1° – 10° for the MC

component. Together, these characteristics argue that the MC component could result from an isothermal remnant magnetization (IRM) imparted by a hand magnet, and the LC component is the same IRM that was subsequently modified viscously by the Earth's field and/or has decayed in our magnetically shielded room before our demagnetization measurements. Equally, it is possible that the MC component could be a blending of the LC component with the magnetization at coercivities higher than the MC component (see following paragraph), where the LC component is an (viscously modified) IRM overprint. This blending behavior is characteristic of AF demagnetization of IRM overprints (Bryson et al., 2023; Vervelidou et al., 2023). Given their lower stabilities, magnetic grains with coercivities in the LC and MC ranges are more likely to have been overprinted by an IRM than grains with coercivities greater than these components. See the [Supplementary Materials](#) for details of the demagnetizations of the LC and MC components.

In contrast, the change in magnetic moment at AF intensities greater than the MC component (18–39 to 120 mT depending on the specimen) is significantly less apparent in the orthogonal projection plots; the points form unstructured clusters close to the origin (Figure 6). Moreover, there is no resolvable loss in moment across this AF range, and the corresponding MAD values (24° – 37° depending on the specimen) are notably larger than those of the LC and MC components. These large MAD values reflect the unstructured nature of the magnetization at coercivities greater than the MC component. Because there is no clear component at these high coercivities, we

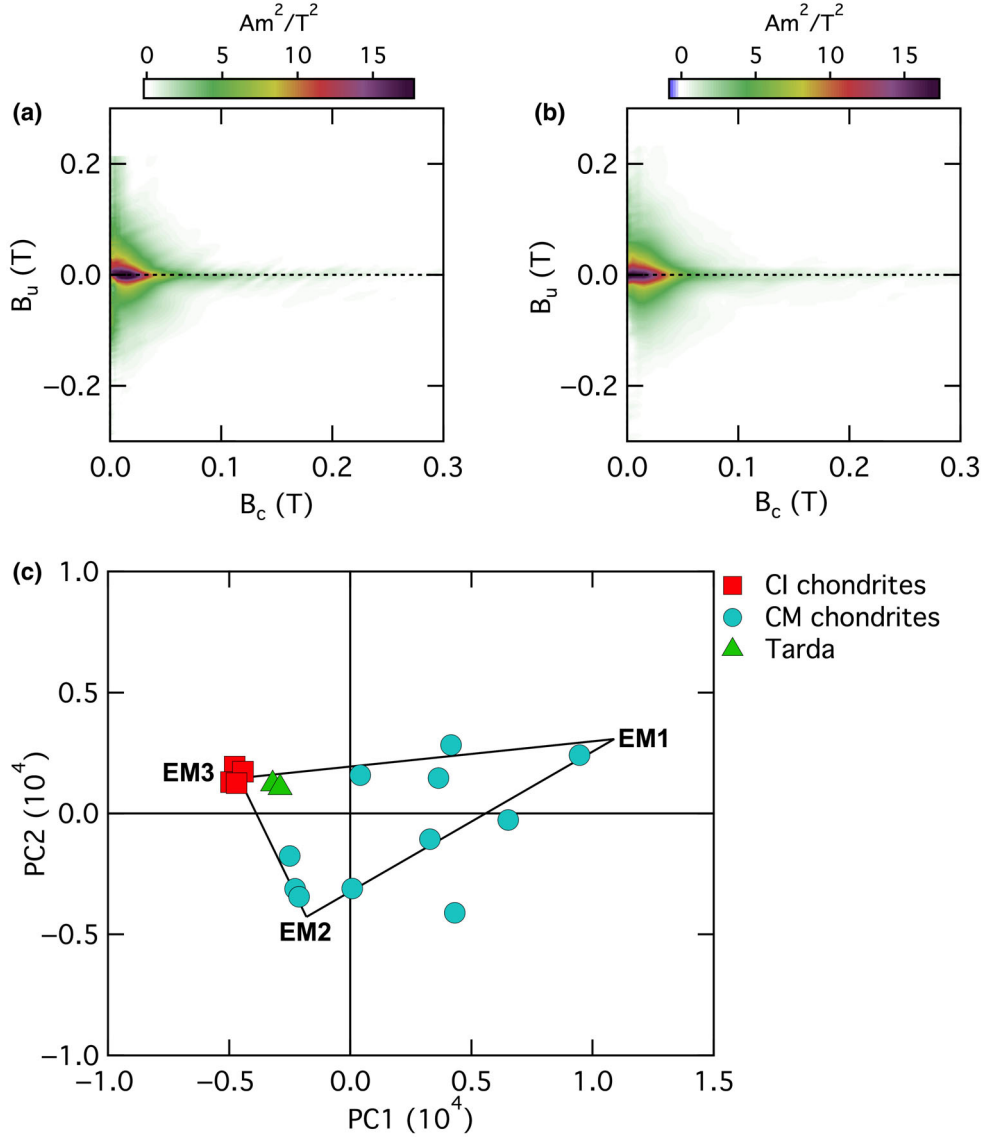


FIGURE 5. (a, b) FORC diagrams of two subsamples of Tarda. (c) PCA of Tarda alongside CI chondrites and CM1.0–1.2 chondrites, including Winchcombe. The black lines represent mixing between three endmembers (EMs) defined by Sridhar et al. (2021).

refrain from calling it a high coercivity component, and instead refer to it as the magnetization at coercivity greater than the MC component. Due to the absence of a clear component, we also chose not to recover a direction of this magnetization using PCA. All these behaviors are expected for a meteorite that experienced an ancient field intensity weaker than the paleomagnetic fidelity of grains with coercivities greater than the MC component. Additionally, this behavior strongly resembles that of the NRM carried by Tagish Lake (Bryson, Weiss, Lima, et al., 2020) and weakly magnetized samples returned from asteroid Ryugu by the Hayabusa2 mission following a

reassessment of their original paleointensities (Maurel et al., 2024; Sato et al., 2022).

We then applied and subsequently AF demagnetized a range of ARMs to each specimen. We chose to do this to both explore the coercivity distribution of their magnetic grains, as well as constrain their paleointensity fidelities and recover paleointensity values where possible through comparisons with the equivalent NRM demagnetizations. The ARMs were mostly demagnetized by an AF intensity of ~ 75 mT (Figure S5), which is greater than the upper limit of the MC component in our specimens (i.e., 18–39 mT). This behavior demonstrates that each specimen

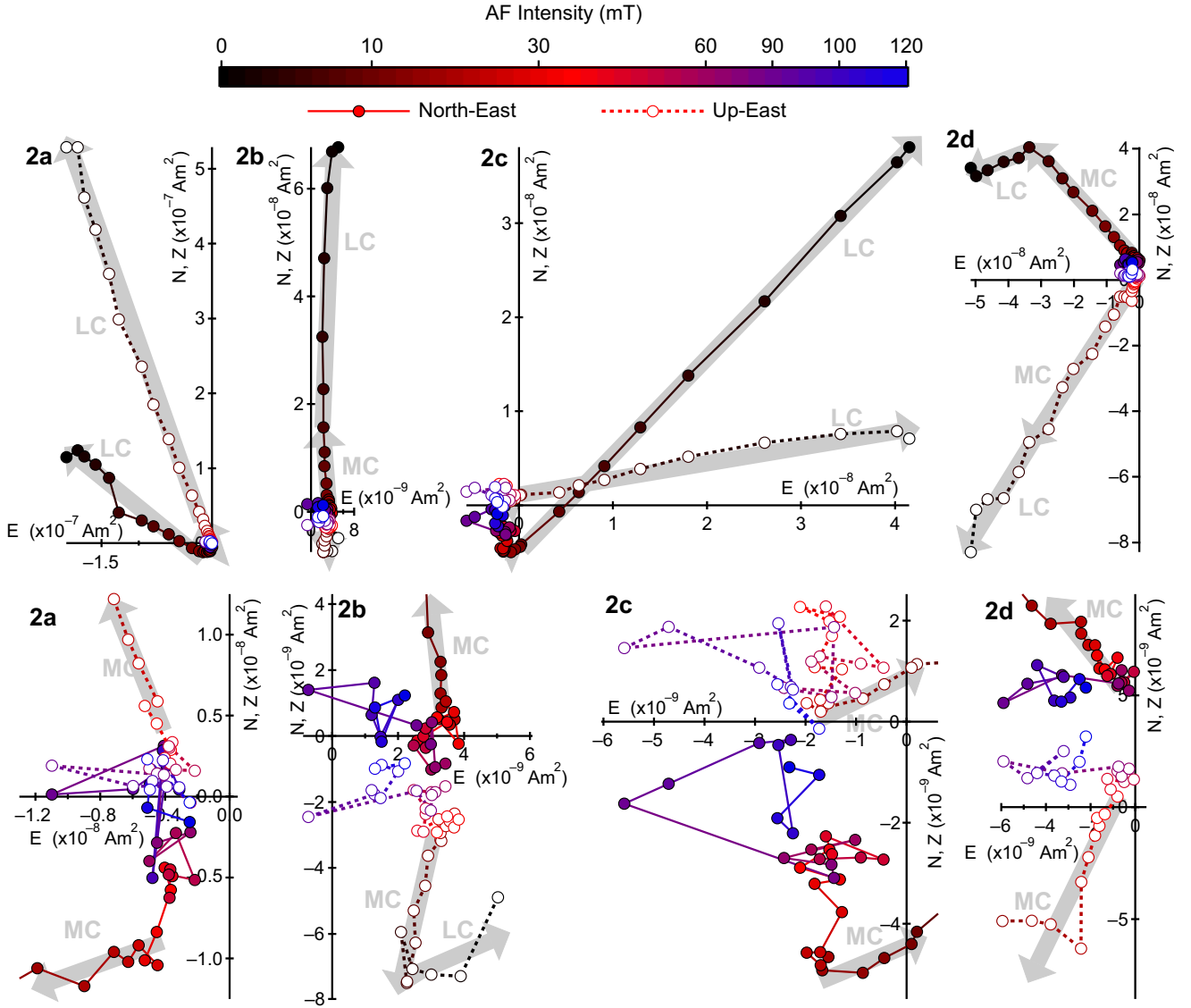


FIGURE 6. Orthogonal projection diagrams of the AF demagnetization of all four specimens of Tarda. The top row shows the complete demagnetization, and the bottom row focusses on AF steps near the origin with weak magnetic moments to highlight the MC component as well as the unstructured nature of the demagnetization at coercivities greater than the MC component.

contains grains with coercivities above the MC component. As such, the lack of a resolvable change during NRM demagnetization at coercivities greater than the MC component argues that Tarda experienced an ancient field intensity weaker than its fidelity limit across this coercivity range, rather than it not containing magnetic grains with coercivities across this range.

To constrain each specimen's paleomagnetic fidelity at coercivities greater than the MC component, we compared the demagnetization of ARMs imparted by a weaker bias field to ARMs imparted by a stronger bias field and attempted to recover the known intensity of the weaker bias field from coercivities greater than the MC component (see the [Supplementary Materials](#) for details). We note that

this approach yields values that are specific to this method and that other methods (e.g., those based on thermal demagnetization) might yield different values. Moreover, our choice of the critical metrics to define high and low fidelity are subjective and could also differ for alternative approaches (see [Supplementary Materials](#)). For the 10 μT ARM (which corresponds to a thermal remanent magnetization [TRM]-equivalent paleointensity of 3 μT given the predominant remanence carrier in Tarda is magnetite; Weiss & Tikoo, 2014), all specimens except of 2a produced fidelity metrics below the critical values (Figure S3). This indicates that 2b, 2c, and 2d were able to record a field with an intensity at least as weak as 3 μT at coercivities greater than the MC component.

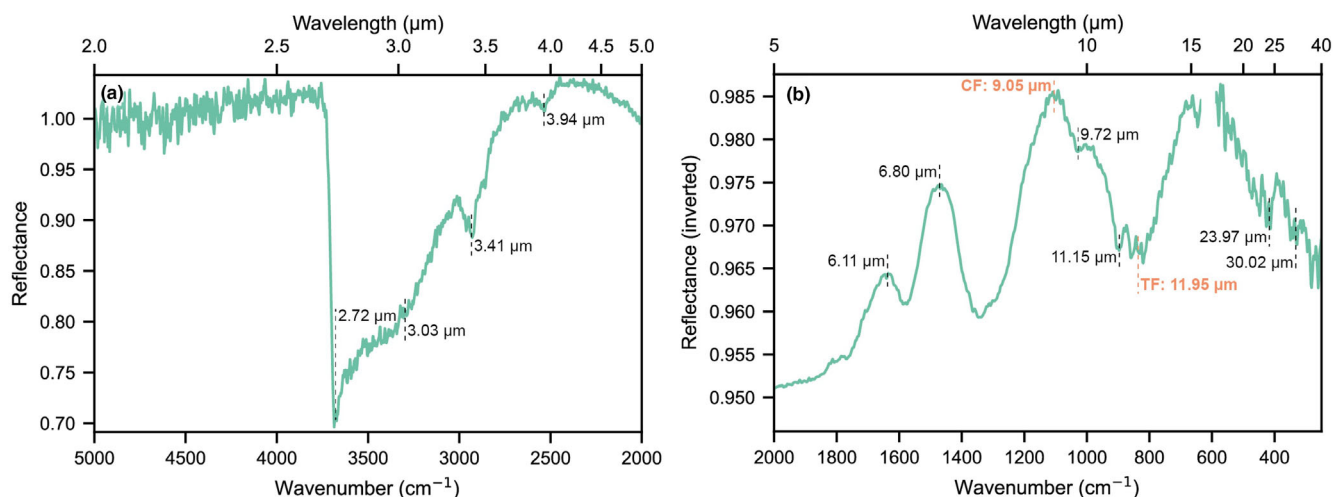


FIGURE 7. (a) Near- and (b) mid-IR reflectance spectra of the bulk homogenized Tarda powder. The positions of key spectral features (e.g., the Christiansen (CF) and Transparency (TF) features) discussed in the main text are highlighted.

For the 1 μT ARM (which corresponds to a TRM-equivalent paleointensity of 0.3 μT), none of the specimens initially yielded fidelity metrics below the critical values, indicating that grains with coercivities greater than the MC component were not able to record fields with intensities as weak as 0.3 μT . However, the demagnetizations of the ARMs and the FORC diagrams indicate that Tarda is only expected to carry a resolvable remanence up to ~ 75 mT (Figures 5 and S5). As such, we expect an NRM could also have only been carried up to ~ 75 mT. Therefore, including the AF demagnetization steps between 75 and 120 mT in our fidelity calculations simply adds noise to the demagnetization sequence, potentially impacting the fidelity metrics. Considering only points between the upper limit of the MC component and 75 mT lowers the fidelity metrics, with those of specimen 2c now falling below the critical values (Figure S3). This suggests that grains with coercivities greater than its MC component in specimen 2c have the potential to have recorded a field at least as weak as 0.3 μT . This is the weakest fidelity value we were able to recover using the ARM setup at the University of Oxford. As such, one of our specimens appears to have the highest fidelity that we were able to determine. Combined with the absence of a clear component at coercivities greater than the MC range, this finding suggests that Tarda experienced a TRM-equivalent ancient field intensity of <0.3 μT (see *Paleomagnetic History* for a discussion on how this value is modified by parent body rotation and uncertainties in CRM acquisition). This is almost identical to the constraints recovered from Tagish Lake, both in terms of intensity (<0.15 μT in Tagish Lake) and fraction of specimens (25% have high fidelity in Tagish Lake) (Bryson, Weiss, Lima, et al., 2020), and is similar to

the constraints recovered from weakly magnetized samples of Ryugu (Maurel et al., 2024). This weak field intensity is also reinforced by paleointensities recovered by comparing the NRM demagnetizations with those of the ARMs (Table S4 and Figure S4), as well as the shapes of the NRM demagnetizations compared to those of the ARMs (Figure S5). Further details on these paleointensities constraints can be found in the [Supplementary Materials](#).

Infrared Spectral Properties

Figure 7 shows the bulk IR reflectance spectra of the Tarda powder between 2 and 40 μm . In the near-IR, there is a feature at ~ 2.72 μm consistent with $-\text{OH}$ in Mg-rich serpentines (Bates et al., 2020; Takir et al., 2013), plus a shoulder near 3.03 μm that is likely due to interlayer H_2O in smectites (Bates et al., 2020) (Figure 7a). Features at ~ 3.41 and ~ 3.94 μm are from organics and carbonates, respectively (Baldrige et al., 2009; Meerdink et al., 2019; Socrates, 2001). In the mid-IR, there are peaks at ~ 6.11 and ~ 6.80 μm (Figure 7b); CI chondrite spectra show a feature near the former that has been linked to smectites (Bates et al., 2020), although we note that organics can also have features in this region (e.g., Socrates, 2001). The feature at ~ 6.80 μm is consistent with the presence of carbonates (Baldrige et al., 2009; Meerdink et al., 2019).

The position of the Christiansen feature (CF) in the mid-IR is related to the optical constants of the constituent minerals within a sample; for Tarda, the CF is at ~ 9.05 μm , comparable to CF positions previously reported for CM chondrites (Figure 7b; Bates et al., 2020; Hanna et al., 2020; Salisbury et al., 1991). In addition, the

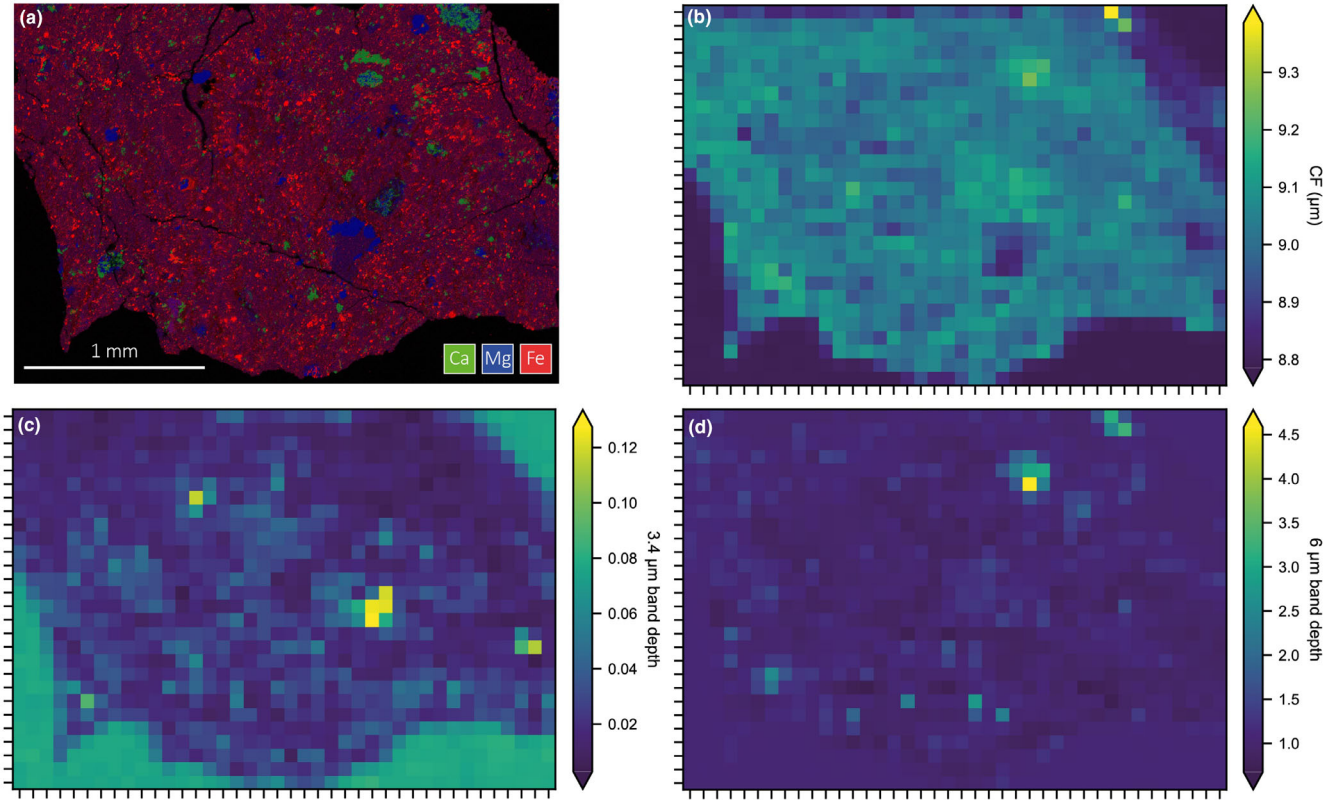


FIGURE 8. (a) Overview EDS map of the smaller polished Tarda sample showing combined calcium (green), magnesium (blue), and iron (red). Micro-IR spectral maps showing variations in the (b) position of the CF, and (c) depth of the 3.4 μm and (d) 6 μm features.

transparency feature (TF), a reflectance maximum caused by a region of optical transparency in fine-grained material, occurs at $\sim 11.95 \mu\text{m}$ in the Tarda spectrum, in agreement with its petrologic subtype of 1.3 (Bates et al., 2023). Vibrational features in the Tarda spectrum at ~ 9.72 , ~ 11.15 , ~ 23.97 , and $\sim 30.02 \mu\text{m}$ are likely from a combination of hydrous and anhydrous silicates, although we note that the latter feature is also consistent with magnetite.

We identified several parameters that varied with the mineralogy and composition of the polished Tarda samples. These included the CF, and the depth of the 3.4 and 6 μm features, both of which are associated with organics and carbonates (Figure 8; Kaplan et al., 2020; Lane & Christensen, 1997; Simon et al., 2020). We find that the position of the CF varies between 8.83 and 9.39 μm across the polished Tarda samples. Figure 8b shows that CFs at shorter wavelengths correspond with areas of the sample that are Mg-rich; individual spectra extracted from these regions display CFs (and vibrational features) that correspond to spectra of Fo_{60–90} olivine (Hamilton, 2010). These observations are consistent with previous micro-IR studies showing that the bulk spectra

of mildly aqueously altered chondrites (i.e., higher olivine abundance) have CFs at shorter wavelengths (Hanna et al., 2020). We also note that the Al-rich chondrule glass (Figure 2d) shows a CF at shorter wavelengths than the material surrounding it.

Figure 8d shows that the depth of the vibrational feature at 6 μm correlates with Ca-rich areas of the polished Tarda sample. This feature is clearly related to largest carbonate grains and shows no significant variation in its spectral position, suggesting that the grains all have a similar composition (i.e., dolomite). In contrast, the 3.4 μm feature is not related to the large carbonate grains and instead shows an increased depth in distinct, porous clasts that appear to contain abundant fine-grained carbonates and silicates (Figure S6). The 3.4 μm feature is thought to result from the symmetric and asymmetric stretching of the C–H bond (e.g., Ehrenfreund et al., 1991), indicating that these clasts are also rich in organics. Furthermore, the clasts show complex reflectance minima near 6 μm (shown as maxima in Figure S6 due to the inverted y-axis) that are not observed elsewhere on the polished Tarda samples.

DISCUSSION

The Conditions and Extent of Alteration

Tarda contains abundant phyllosilicates (~72 vol%) and few anhydrous silicates (~10 vol%), resulting in a petrologic subtype of 1.3 on the scale of Howard et al. (2015). The bulk mineralogy indicates that Tarda's parent body (or at least a region of the parent body) underwent aqueous alteration that was extensive but did not reach completion. In agreement with other studies (e.g., Chennaoui Aoudjehane et al., 2021; Gattacceca et al., 2021; Marrocchi et al., 2021), we find chondrule fragments and individual silicate grains in the matrix of Tarda that most likely represent the initial unaltered mineralogy of the parent body (Figure 2a). The high degree of aqueous alteration is supported by Tarda's bulk water abundance (~12.5 wt% estimated from TGA, Figure 4 and Table S2; ~8.5 wt% by mass spectrometry, Marrocchi et al., 2021) and the shape and position of the 3 μm absorption band, and TFs and CFs in IR spectra (Figure 7; Yesiltas et al., 2022).

Phyllosilicates in Tarda are Mg-rich serpentine and smectite, similar to other highly altered chondrites and extraterrestrial samples, and reflect the progressive hydration of increasingly Mg-rich silicates (e.g., Russell et al., 2022). Bulk XRD indicates that the carbonates are predominantly dolomite, which would have precipitated from chemically evolved fluids produced by the extensive water–rock reactions (e.g., Endress & Bischoff, 1996; Lee et al., 2014). Magnetite is abundant in Tarda and mainly occurs as framboids, although plaquettes and spherules are also observed, with the variation in morphologies possibly related to changes in the supersaturation of the aqueous fluids (e.g., Ono et al., 2024). Magnetite is thought to form early in alteration sequences from the oxidation of metal and amorphous silicates (e.g., Palmer & Lauretta, 2011), but the presence of magnetite pseudomorphs of coarse-grained Fe-sulfide grains suggests at least one late-stage alteration event (Figure 3c; Zolensky et al., 2002). The replacement of coarse (>5 μm) Fe-sulfide grains is consistent with their relatively low abundance (0.2 ± 0.1 area%) in the polished samples; however, the high bulk Fe-sulfide abundance (~8 vol%) determined by PSD-XRD, which can detect grains that are <5 μm in size, hints at a final stage of sulfide deposition (Zolensky et al., 2002). Based on the composition of Fe-sulfide grains, Schrader et al. (2022) estimated that Tarda was altered at temperatures of <150°C, which is consistent with its phyllosilicates showing no evidence for significant heating.

In summary, Tarda records water–rock reactions on a parent body that must have accreted at least beyond the water snowline, possibly even further out (e.g., Marrocchi

et al., 2021), in the early solar system. These reactions were extensive, which is reflected in the abundance and composition of Tarda's phyllosilicates and carbonates, but did not reach completion, with some of the original mineralogy still preserved as unaltered or partially altered chondrule fragments. The geological sequence of alteration on Tarda's parent body was also likely complex, with multiple episodes of magnetite, carbonate, and Fe-sulfide formation.

Relationship to Tagish Lake, WIS 91600, and MET 00432

The petrographic and geochemical properties of Tarda presented both here and in other studies are consistent with a classification as a C2-ung carbonaceous chondrite (Chennaoui Aoudjehane et al., 2021; Gattacceca et al., 2021). However, its secondary mineral assemblage and bulk light element isotopic compositions indicate that Tarda is closely related to Tagish Lake, ~10 kg of which was recovered soon after being seen to fall in Canada in 2000 (Brown et al., 2000). Tagish Lake is a C2-ung breccia comprised of several lithologies, namely distinct carbonate-rich and carbonate-poor lithologies (e.g., Zolensky et al., 2002), and previous XRD studies have reported a wide range of mineral abundances: 3–40 vol% olivine (average ~19 vol%), 0–13 vol% pyroxene (av. ~3 vol%), 4–21 vol% magnetite (av. ~11 vol%), 0–15 vol% Fe-sulfide (pyrrhotite + pentlandite, av. ~7 vol%), 6–21 vol% carbonates (calcite + dolomite + siderite, av. ~11 vol%), 0–11 vol% sulfates (av. ~2 vol%), and 11–72 vol% phyllosilicates (serpentine + smectite, av. ~52 vol%) (Gilmour et al., 2019; Izawa et al., 2015). Bland et al. (2004) determined the bulk mineralogy of Tagish Lake using the same PSD-XRD setup employed in this study, and there is good agreement between their mineral abundances (71 vol% phyllosilicate, 7 vol% olivine, and 5 vol% each of magnetite and sulfide) and our values for Tarda (Table S1). The only exception is for the carbonates, with Bland et al. (2004) potentially sampling a carbonate-rich lithology (12 vol%). XRD patterns and bulk mineral abundances, therefore, offer further support for a link between Tarda and Tagish Lake. Similarly, TGA data sets for Tarda presented both here and in Yesiltas et al. (2022) are consistent with those acquired from five aliquots of Tagish Lake by Gilmour et al. (2019) (Table S2).

Tarda has been described as a breccia (Chennaoui Aoudjehane et al., 2021; Gattacceca et al., 2021), although our polished sections appear to sample only a single lithology (Figure 1). Nevertheless, we concur that intact chondrules (or chondrule pseudomorphs) and CAIs are relatively rare in Tarda (e.g., Marrocchi et al., 2021; Morin et al., 2022; Yesiltas et al., 2022) and that its petrographic characteristics are similar to Tagish Lake (e.g., Brown

et al., 2000; Zolensky et al., 2002). In particular, magnetite framboids are widespread throughout the matrix of Tarda and Tagish Lake, while both meteorites contain examples of magnetite framboid pseudomorphs of coarse Fe-sulfide grains (Figure 3; Yamanobe et al., 2018; Zolensky et al., 2002).

The IR reflectance spectrum of Tagish Lake suggests that it could sample a primitive D-type asteroid that formed in the outer regions of the solar system (Hiroi et al., 2001). A potential link with D-type asteroids has also been proposed for the carbonaceous chondrites Meteorite Hills (MET) 00432 (CM2) (Nakamura et al., 2013) and WIS 91600 (Hiroi et al., 2005). MET 00432 contains phyllosilicates (serpentine + smectite, 83 vol%), magnetite (8 vol%), including abundant framboids, and minor (≤ 5 vol%) anhydrous silicates (olivine + pyroxene), Fe-sulfides (pyrrhotite + pentlandite), and carbonates (dolomite) (Howard et al., 2015; Nakamura et al., 2013; Yamanobe et al., 2018). It has a bulk oxygen isotopic composition similar to Tagish Lake and Tarda, but the abundance and size of chondrules and composition of carbonates in MET 00432 is different (Nakamura et al., 2013). WIS 91600 also has an oxygen isotopic composition similar to Tagish Lake and Tarda (Choe et al., 2010) and contains serpentine and smectite (~ 80 vol%), framboidal, plaquette and spherulitic magnetite (> 5 vol%, Bates et al., 2021; Howard et al., 2015; King et al., 2021), and magnetite pseudomorphs of Fe-sulfide grains (Tonui et al., 2014); however, chondrules and CAIs are relatively common in WIS 91600 relative to Tagish Lake and Tarda (Biryukov & Ulyanov, 1996; Brearley, 2004; Render et al., 2022; Yamanobe et al., 2018). Furthermore, phyllosilicates in WIS 91600 were dehydrated by a short-lived metamorphic event at temperatures of ~ 400 – 500°C (Bates et al., 2021; Choe et al., 2010; King et al., 2021; Tonui et al., 2014; Yabuta et al., 2010), indicating a different alteration history to Tagish Lake and Tarda, although we note that Northwest Africa (NWA) 12563 (CM2-an) may represent material similar to the unheated precursor of WIS 91600 (Hewins et al., 2021).

Paleomagnetic History

Despite a pronounced terrestrial overprint (carried by the LC and MC components), we were able to identify and isolate the pre-terrestrial remanence carried by Tarda (carried at coercivities greater than the MC range). This remanence is very weak, consistent with an ancient field intensity of $< 0.3 \mu\text{T}$, which is very similar to that recovered from Tagish Lake ($< 0.15 \mu\text{T}$; Bryson, Weiss, Lima, et al., 2020) and weakly magnetized samples of Ryugu (Maurel et al., 2024). Following the same arguments as those outlined for Tagish Lake (Bryson, Weiss, Lima, et al.,

2020), the magnetic remanence carried by Tarda is expected to be a chemical remanent magnetization (CRM) recorded as magnetite formed. Extending both the Mn-Cr ages of carbonates (~ 3 – 4 Myr after CAI formation; Fujiya et al., 2013) and the sequence in which alteration phases formed (i.e., magnetite was one of the earlier products of aqueous alteration; Zolensky et al., 2002) from Tagish Lake to Tarda, it is likely that magnetite formed sometime between ~ 3 and 3.5 Myr after CAI formation in Tarda. This is similar to the magnetite formation and CRM acquisition age in CM chondrites (~ 3.5 Myr; Bryson et al., 2023; Suttle et al., 2021), arguing that Tarda experienced the same magnetic field as the CM chondrites as its magnetite formed. This field is thought to be that carried by the protoplanetary disk (Bryson et al., 2023), which has also been argued to be the case for Tagish Lake (Bryson, Weiss, Lima, et al., 2020). We therefore expect the CRM carried by Tarda to reflect the local properties of this field at the location that its parent body formed and underwent aqueous alteration.

To recover this local field intensity, the influence of several features on Tarda's paleointensity need to be accounted for, namely, parent body rotation; the recording efficiency of CRMs relative to TRMs; the recording efficiency of different morphologies of magnetite; and the natural decay of paleomagnetic remanence over billions of years. For the case of parent body rotation, the time scales of magnetite formation were almost certainly longer than the rotation period of the Tarda parent body, meaning that Tarda will have recorded a time-average of the disk field projected onto the rotation axis of its parent body. Accounting for the average possible angle of this tilt, this time-averaging causes the paleointensity recorded by a meteorite to be on average half that of the background field (Fu et al., 2014). As such, accounting for this effect, the local disk field at the Tarda parent body was most likely $< 0.6 \mu\text{T}$.

A recent experimental study exploring the recording efficiency of CRMs relative to TRMs (Maurel & Gattacceca, 2023) found that paleointensities recovered from CRMs may need to be multiplied by a factor of 1.9 – 3.2 to recover TRM-equivalent values. However, this factor was determined from experiments involving magnetite formation through pseudomorphic replacement of pyrite. While this reaction involves a nonmagnetic parent phase, it does not reflect the predominant magnetite formation mechanisms of magnetite in Tarda, which is precipitation. CRM recording efficiency depends heavily on the formation reaction/pathway (e.g., Ge et al., 2021; Jiang et al., 2017). As such, the applicability of this value to Tarda is unclear. Another recent study argues that the CRM to TRM conversion factor is ~ 1 – 1.4 for magnetite precipitation over time scales of 10^4 – 10^5 years (Baker & Muxworthy, 2023), while original studies proposed a value

of $\sim 1\text{--}2$ for alteration time scales of 10^5 years (e.g., McClelland, 1996). However, these studies are theoretical and idealized, so may not capture some of the nuances that occurred during magnetite formation in complex geological material such as Tarda. Bearing all of this mind, we chose to adopt a nominal factor of 1 because it captures the relevant formation mechanism of magnetite and produces paleointensities that are directly comparable to previous studies (e.g., Bryson et al., 2023; Bryson, Weiss, Lima, et al., 2020; Cournède et al., 2015). However, we also consider a value of 2 because this overlaps for the lower and upper end of the range proposed by Maurel and Gattacceca (2023) as well as the upper end of the range proposed by McClelland (1996).

For the case of magnetite morphologies, Bryson et al. (2023) argue that magnetite that formed via precipitation (e.g., framboids and plaquettes) is able to record a reliable CRM during this process. Since precipitative magnetite is by far the most common magnetite morphologies in Tarda (Figures 3 and 5), we assume that the recording efficiency of magnetite in this meteorite is 1.

For the case of natural remanence decay, Nagy et al. (2017) found that magnetite particles >110 nm adopt vortex domain states, which are able to preserve a magnetic remanence for longer than the age of the solar system. The predominant paleomagnetic carrier in Tarda are framboids and plaquettes of magnetite, the constituent grains of which are >110 nm in size (Figure 3), and previous studies have shown that grains in framboidal magnetite adopt vortex domain states (Kimura et al., 2013). As such, we do not expect significant natural decay in remanence carried by Tarda over the lifetime of the solar system.

Accounting for parent body rotation, CRM recording efficiency, magnetite morphologies, and the natural remanence decay, the field experienced by Tarda was most likely <0.6 μT , and we consider the possibility that it was <1.2 μT . Following the same arguments as Bryson, Weiss, Lima, et al. (2020), we do not believe that the Verwey transition, nor a tumbling parent body, nor very high tilt angles of the rotation axis of the parent body are the likely causes of the weak remanence recorded by Tarda.

In a broad sense, Tarda's thermal and aqueous histories are similar to that experienced by most CM chondrites (Suttle et al., 2021) and Tagish Lake (Zolensky et al., 2002), indicating that these meteorites recorded directly comparable magnetic remanences. Our recovered paleointensity for Tarda (nominally <0.6 μT) is significantly weaker than the paleointensity recovered from CM chondrites, which is ~ 78 μT accounting for the recording efficiencies of different magnetite morphologies and parent body tilt in CM chondrites (Bryson et al., 2023; Cournède et al., 2015). Given the concordance in CRM

acquisition ages of Tarda and CM chondrites, this difference most likely reflects different formation locations of the Tarda parent body compared to that of CM chondrites in the protoplanetary disk. Models of the disk's magnetic field indicate that the intensity of its field decreased with heliocentric distance from the Sun as the density of dust and gas decreased (Weiss et al., 2021). The weaker paleointensity recorded by Tarda relative to CM chondrites therefore suggests that the Tarda parent body formed further from the Sun than that of the CM chondrites. Specifically, adopting the same field intensity profile as Bryson, Weiss, Lima, et al. (2020), we calculate a formation distance of the Tarda parent body of >8.3 AU, although this is based on several assumptions regarding the nature of the disk field (e.g., monotonically decreasing density profile throughout the disk; uniform accretion rates in different reservoirs of the disk; Borlina et al., 2021). Using a CRM recording efficiency factor of 2, this formation distance becomes >5.4 AU.

A formation distance for Tarda of $>5.4\text{--}8.3$ AU is similar to that proposed for Tagish Lake (i.e., notably more distal than the CM chondrite parent body, with a possible quantitative constraint of $>8\text{--}13$ AU; Bryson, Weiss, Lima, et al., 2020). Following the same arguments as Tagish Lake (Bryson, Weiss, Lima, et al., 2020), the presence of chondrule fragments in Tarda suggests that these solids were able to migrate beyond the formation reservoir of typical carbonaceous chondrites in just a few million years, supporting the particularly efficient migration of mm-sized objects throughout the protoplanetary disk as observed in returned samples from comet 81P/Wild2 (Brownlee et al., 2006).

Multiscale Spectral Observations

It is critical to combine spectral observations over multiple spatial scales. A case where this is particularly relevant is the diagnostic CF, which is directly related to the optical properties of minerals. In complex materials such as meteorites, the CF tends to be a combination of the individual CFs of each mineral present (Salisbury et al., 1991). Previous studies of carbonaceous chondrite spectra have highlighted differences in how the CF behaves with the degree of aqueous alteration. For example, Bates et al. (2020) showed the CF shifting to shorter wavelengths with increasing aqueous alteration, in contrast to the trend reported by Hanna et al. (2020). These studies analyzed carbonaceous chondrite samples prepared in different ways—powders and polished sections—but this alone cannot explain the discrepancy in the observed CF trends.

Here, our in situ micro-IR spectra enable us to target specific minerals in Tarda regardless of its bulk degree of aqueous alteration, allowing us to interpret variations in

the CF position. We find that CFs at shorter wavelengths correspond to both Mg-rich anhydrous silicates (e.g., forsteritic olivine) and phyllosilicates (Figure 8) and, therefore, propose that the previously reported differences in CF trends are because Bates et al. (2020) investigated CM chondrites of petrologic type 1.2 and 1.1, whereas Hanna et al. (2020) analyzed samples over a wider petrologic range (1.6–1.2) but did not include the most aqueously altered chondrites. The least altered CM chondrites contain a higher fraction of anhydrous silicates, resulting in spectra with CFs at shorter wavelengths (Hanna et al., 2020). Similarly, the most altered CM chondrites contain abundant Mg-rich phyllosilicates, which also have CFs at shorter wavelengths. As such, intermediately altered CM chondrites with few (typically <20 vol%) anhydrous silicates and relatively high Fe/Mg ratios show CFs at the longest wavelengths (Bates et al., 2020).

The detection of carbonates also benefits from a combined approach of bulk and micron scale observations. Carbonates have a number of spectral features of interest, including the ν_3 (third fundamental) absorption at ~ 6.35 to $6.75 \mu\text{m}$ and the narrow ν_2 fundamental absorption near $11.4 \mu\text{m}$. The micro-IR spectral maps clearly show both carbonate features; ν_3 absorptions between 6.97 and $7.08 \mu\text{m}$ and ν_2 absorptions between 11.42 and $11.45 \mu\text{m}$ (Figure S7). In comparison, the bulk spectrum of Tarda has a feature at $6.80 \mu\text{m}$ that is consistent with carbonate, but we do not observe the ν_2 fundamental absorption, likely because of the high abundance of phyllosilicates (>70 vol%), which have strong features in this spectral region (Figure 7b). The detection of carbonates on hydrated asteroid surfaces, therefore, cannot be ruled out based on the absence of the ν_2 absorption, especially if the abundance is low (e.g., ~ 2 vol% for Tarda) relative to phyllosilicates.

Recently, NASA's OSIRIS-REx mission characterized the surface mineralogy of the near-Earth carbon-rich asteroid (101955) Bennu using visible IR (OVIRS, 0.4 – $4.3 \mu\text{m}$) and thermal emission (OTES, ~ 5.71 – $100 \mu\text{m}$) spectrometers (e.g., Hamilton et al., 2019). No spectral features definitively associated with carbonates were identified in the global spectrum of Bennu collected by OTES, which had a spatial resolution of 20 – 40 m. However, VNIR spectra acquired at higher spatial resolution (4×9 m) showed features near $3.4 \mu\text{m}$ that were attributed to bright carbonate veins on Bennu's surface (Kaplan et al., 2020). The OTES signal to noise is described as “low” at wavelengths below $\sim 7.4 \mu\text{m}$ (Kaplan et al., 2020), potentially masking the ν_3 absorption. Furthermore, as we have shown here, bulk “global” spectra of asteroids are unlikely to show the ν_2 absorption spectral features unless the abundance of carbonate is relatively high (at least >2 vol%). Based on

the remote observations, we predict that Bennu's surface has a bulk carbonate abundance of only a few vol%, which appears to be consistent with preliminary analysis of the returned materials (e.g., Lauretta et al., 2024). We anticipate that reflectance spectra acquired from Tarda will also be useful for ground truthing upcoming observations of Jupiter's Trojans and the Martian moon Phobos by the Lucy and MMX missions, respectively.

Organic-Rich Clasts

Although carbonates show absorptions near $3.4 \mu\text{m}$ (Calvin et al., 1994; Rivkin et al., 2006), this feature is usually associated with aliphatic organics (e.g., Ehrenfreund et al., 1991; Kebukawa et al., 2011; Yesiltas & Kebukawa, 2016). The deepest $3.4 \mu\text{m}$ features in our micro-IR spectral maps of Tarda are correlated with distinct, porous clasts that contain abundant fine-grained carbonates and silicates. These clasts are somewhat similar to the “dark, granular clasts” identified in a polished section of Tarda by Yesiltas et al. (2022), who described them as hosting organic matter. Spectra extracted from the clasts also show features between 5 and $7 \mu\text{m}$ from fine-grained silicates (e.g., Bates et al., 2020), organics (e.g., Kebukawa et al., 2011), and carbonates. Carbonate features in spectra from other regions of the samples are typically single reflectance maximum (minimum as plotted) close to $7 \mu\text{m}$ (Figure S7), whereas spectra from the clasts display multiple reflectance minima (maxima as plotted, Figure S7), potentially due to volume scattering from the porous texture.

To further evaluate the causes of the complex 3.4 and $6 \mu\text{m}$ features, Gaussian curves (Figure 9) were used to fit the spectra shown in Figures S6 and S7. The two spectral regions were normalized to a linear continuum fit between two points 3.2 and $3.6 \mu\text{m}$, and 5.2 and $7.5 \mu\text{m}$. The $3.4 \mu\text{m}$ feature has contributions from individual features near 3.36 , 3.40 , 3.48 , and $3.50 \mu\text{m}$, which are consistent with the CH_3 asymmetric, CH_2 asymmetric, CH_3 symmetric, and CH_2 symmetric vibrational modes, respectively (Socrates, 2001). Based on the method of Quirico et al. (2018), a CH_2/CH_3 ratio of 1.00 ± 0.01 was determined by comparing the relative peak intensities at 3.38 and $3.42 \mu\text{m}$ from all spectra extracted from the porous clasts. In the $6 \mu\text{m}$ region, there are six contributions; at 5.53 , 5.79 , 6.14 , 6.51 , 6.82 , and $7.19 \mu\text{m}$, some of which are likely due to silicate minerals. For example, spectra of forsteritic olivine show features between 5.65 and $6.00 \mu\text{m}$, and saponite has features near 5.89 – $6.17 \mu\text{m}$ (Bates et al., 2020). However, the feature at $6.14 \mu\text{m}$ is approximately where $\text{C}=\text{C}$ stretching vibrational features occur (usually near 6.16 – $6.33 \mu\text{m}$, Socrates, 2001), while the feature near $6.82 \mu\text{m}$ is

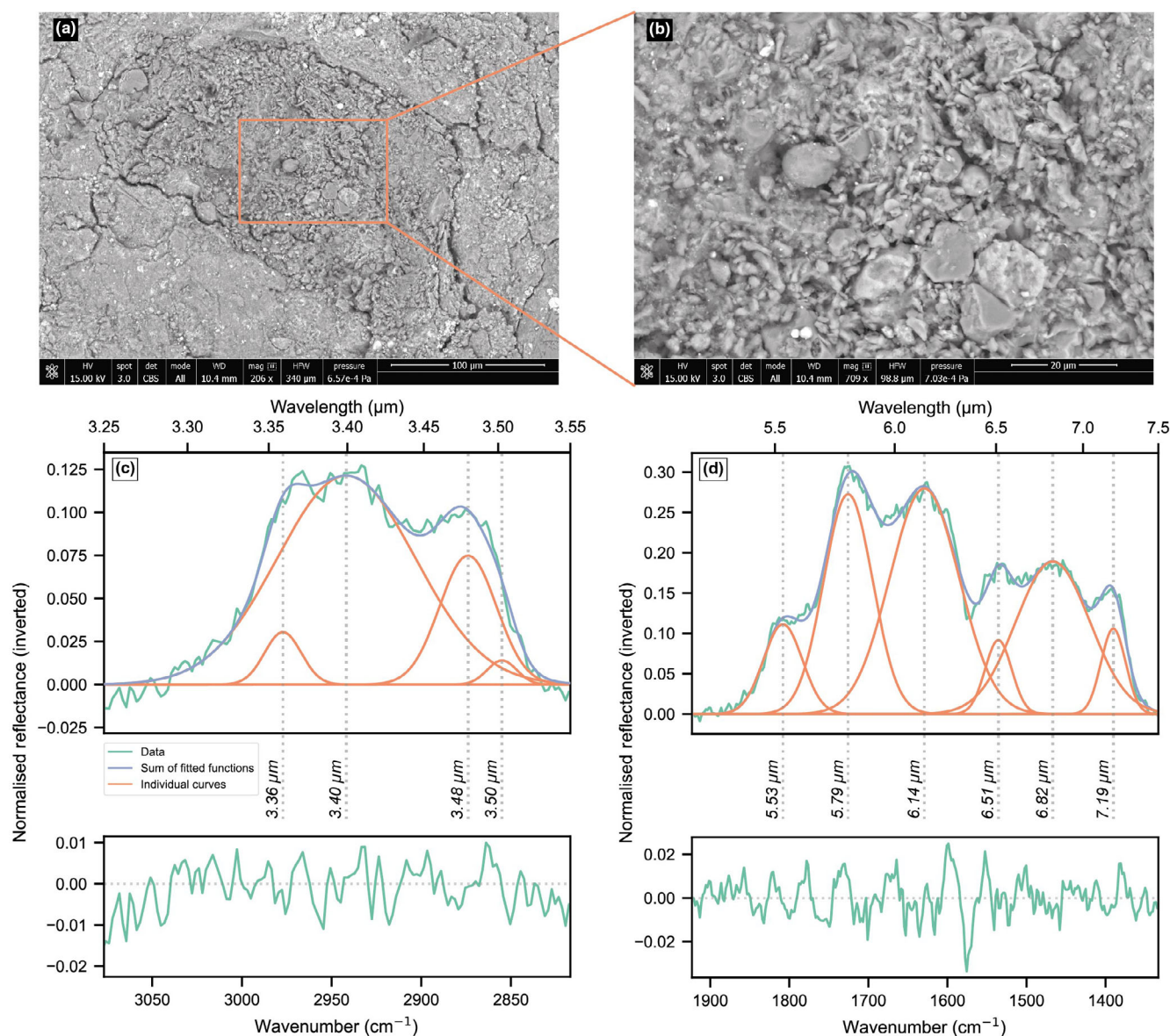


FIGURE 9. (a, b) BSE images of porous clasts containing abundant fine-grained carbonates and silicates in the Tarda meteorite, and fitting procedure and residuals (bottom panels, spectra minus the sum of the fitted function) for the (c) 3.4 μm and (d) 6 μm features.

consistent with asymmetric bending of CH_3 (6.82–6.90 μm, Socrates, 2001). In addition, the small feature near 7.19 μm could result from symmetric bending of CH_3 (usually 7.25–7.27 μm, Socrates, 2001), although fine-grained carbonate also shows reduced spectral contrast in this region (relative to coarse and solid sample spectra), with a small minimum (maximum as plotted) near 7.25 μm (Baldrige et al., 2009; Meerdink et al., 2019).

We conclude that both the 3.4 and 6 μm features in spectra from the porous clasts in Tarda are consistent with the presence of aliphatic-rich organics. The CH_2/CH_3 ratio of the clasts (1.00 ± 0.01) is lower than

that reported for insoluble organic matter (IOM) extracted from the CI chondrites (1.15–1.30), Tagish Lake (1.45–1.80), and WIS 91600 (2.60) (Kebukawa et al., 2011; Orthous-Daunay et al., 2013; Quirico et al., 2018). A low CH_2/CH_3 ratio likely indicates shorter aliphatic chain lengths and/or higher branching levels (Flynn et al., 2003), and is thought to possibly reflect an interstellar composition (Kebukawa et al., 2011). The CH_2/CH_3 ratio for WIS 91600 has been attributed to thermal metamorphism (Orthous-Daunay et al., 2013; Quirico et al., 2018), whereas the relatively high values for Tagish Lake may indicate a depletion in aliphatic

groups due to extensive chemical oxidation and carbonate precipitation (Cody & Alexander, 2005). We suggest that the porous clasts in Tarda record lower levels of alteration than Tagish Lake, and therefore preserve the pristine composition, with a potentially interstellar component, of the parent body prior to extensive water-rock reactions.

CONCLUSIONS

Tarda is an ungrouped, hydrated carbonaceous chondrite that resembles the Tagish Lake (C2-ung) meteorite, which has been linked to dark D-type asteroids thought to sample primitive conditions in the outer regions of the solar system. Here, we describe the nature and extent of alteration, paleomagnetic history, and IR spectral properties of the Tarda meteorite. We find that:

- 1.. Tarda consists of abundant (>70 vol%) Mg-rich phyllosilicates (serpentine and smectite), magnetite, sulfides (pyrrhotite), and carbonates (dolomite), and has a bulk water content of ~12.5 wt% (based on TGA). Anhydrous silicates are present in chondrule fragments and isolated grains in the matrix but are relatively rare (≤ 10 vol%), while no CAIs were identified. The mineralogy and petrography indicate that Tarda's parent body experienced low temperature (<150°C) aqueous alteration that was extensive but did not reach completion.
- 2.. Magnetite is the primary magnetic phase in Tarda; it is typically framboidal in morphology and found as clusters of either small (<1 μm) grains or larger (>1 μm) individual grains in the matrix. FORC diagrams of Tarda are very similar to those previously reported for WIS 91600 (Bryson, Weiss, Biersteker, et al., 2020) and the CI chondrites (Sridhar et al., 2021) suggesting that these meteorites share almost identical magnetic mineralogies (i.e., size, proximities, morphologies, and arrangements of magnetite grains) and, therefore, a common formation pathway.
- 3.. Tarda's pre-terrestrial paleomagnetic remanence is similar to that of Tagish Lake, with both meteorites likely recording magnetizations when the protoplanetary disk and its magnetic field were still present. This remanence is also similar to that recovered from a recent study of Ryugu (Maurel et al., 2024). For Tarda, this paleointensity is weaker than the lower limit that we were able to recover using our experimental set-up (i.e., <0.6 μT). This paleointensity argues that Tarda's parent body formed more distally than that of the CM chondrites, possibly >5.4–8.3 AU.
- 4.. Tarda retains distinct, porous clasts that contain aliphatic-rich organics. The CH_2/CH_3 ratio of the clasts (1.00 ± 0.01) determined from micro-IR spectra is lower than those reported for IOM extracted from Tagish Lake, WIS 91600, and CI chondrites and consistent with an interstellar origin. The clasts likely preserve the pristine composition of Tarda's parent body prior to any significant water-rock reactions taking place.
- 5.. Together, the XRD patterns, bulk mineral abundances, TGA and IR data sets, and paleomagnetic properties suggest a genetic relationship between Tarda and Tagish Lake. This supports previous studies that first proposed a link based on bulk chemical and isotopic compositions.

Acknowledgments—We would like to thank Jens Najorka, Tobias Salge, Innes Clatworthy, and Wren Montgomery for ensuring that the XRD, SEM, and IR instruments used in this study continue to run smoothly. Jérôme Gattacceca, an anonymous reviewer, and Yves Marrocchi are thanked for helpful comments that improved the manuscript. HCB and AJK acknowledge funding through UK Research and Innovation (UKRI) grant number MR/T020261/1; CSH and EB-H are funded by the Science and Technology Facilities Council (STFC). JFJB acknowledges funding through UKRI grant number EP/Y014375/1.

Conflict of Interest Statement—The authors declare that there are no conflicts of interest.

Data Availability Statement—The data that support the findings of this study are available from the corresponding author upon reasonable request.

Editorial Handling—Dr. Yves Marrocchi

REFERENCES

- Alexander, C. M. O'D., Bowden, R., Fogel, M. L., Howard, K. T., Herd, C. D. K., and Nittler, L. R. 2012. The Provenances of Asteroids, and their Contributions to the Volatile Inventories of the Terrestrial Planets. *Science* 337: 721–23.
- Alfing, J., Patzek, M., and Bischoff, A. 2019. Modal Abundances of Coarse-Grained (>5 μm) Components within CI-Chondrites and their Individual Clasts—Mixing of Various Lithologies on the CI Parent Body(ies). *Geochemistry* 79: 125532.
- Avicé, G., Meier, M. M. M., and Marrocchi, Y. 2022. Origin of Radiogenic ^{129}Xe Variations in Carbonaceous Chondrites. *Geochemical Perspectives Letters* 23: 1–4.
- Baker, E. B., and Muxworthy, A. R. 2023. Using Preisach Theory to Evaluate Chemical Remanent Magnetization and its Behaviour during Thellier-Thellier-Coe Paleointensity Experiments. *Journal of Geophysical Research: Solid Earth* 128: e2022JB025858.

- Baldrige, A. M., Hook, S. J., Grove, C. I., and Rivera, G. 2009. The ASTER Spectral Library Version 2.0. *Remote Sensing of Environment* 113: 711–15.
- Bates, H. C., Donaldson Hanna, K. L., King, A. J., Bowles, N. E., and Russell, S. S. 2021. A Spectral Investigation of Aqueously and Thermally Altered CM, CM-an, and CY Chondrites under Simulated Asteroid Conditions for Comparison with OSIRIS-REx and Hayabusa2 Observations. *Journal of Geophysical Research: Planets* 126: e2021JE006827.
- Bates, H. C., King, A. J., Donaldson Hanna, K. L., Bowles, N. E., and Russell, S. S. 2020. Linking Mineralogy and Spectroscopy of Highly Aqueously Altered CM and CI Carbonaceous Chondrites in Preparation for Primitive Asteroid Sample Return. *Meteoritics & Planetary Science* 55: 77–101.
- Bates, H. C., King, A. J., Shirley, K. S., Bonsall, E., Schröder, C., Wombacher, F., Fockenberg, T., Curtis, R. J., and Bowles, N. E. 2023. The Bulk Mineralogy, Elemental Composition, and Water Content of the Winchcombe CM Chondrite Fall. *Meteoritics & Planetary Science* 59: 1006–28. <https://doi.org/10.1111/maps.14043>.
- Biryukov, V. V., and Ulyanov, A. A. 1996. Petrology and Classification of New Antarctic Carbonaceous Chondrites PCA91082, TIL91722, and WIS91600. *Proceedings of the NIPR Symposium on Antarctic Meteorites* 9: 8–19.
- Bland, P. A., Cressey, G., and Menzies, O. N. 2004. Modal Mineralogy of Carbonaceous Chondrites by X-Ray Diffraction and Mössbauer Spectroscopy. *Meteoritics & Planetary Science* 39: 3–16.
- Borlina, C. S., Weiss, B. P., Bryson, J. F. J., Bai, X.-N., Lima, E. A., Chatterjee, N., and Mansbach, E. N. 2021. Paleomagnetic Evidence for a Disk Substructure in the Early Solar System. *Science Advances* 7: eabj6928.
- Brearley, A. J. 2004. A Unique Style of Alteration of Iron-Nickel Metal in WIS 91600, an Unusual C2 Carbonaceous Chondrite. *35th Lunar & Planetary Science Conference*, abstract #1358.
- Brown, P. G., Hildebrand, A. R., Zolensky, M. E., Grady, M., Clayton, R. N., Mayeda, T. K., Tagliaferri, E., et al. 2000. The Fall, Recovery, Orbit, and Composition of the Tagish Lake Meteorite: A New Type of Carbonaceous Chondrite. *Science* 290: 320–25.
- Brownlee, D., Tsou, P., Aléon, J., Alexander, C. M. O'D., Araki, T., Bajt, S., Baratta, G. A., et al. 2006. Comet 81P/Wild 2 under a Microscope. *Science* 314: 1711–16.
- Bryson, J. F. J., Nichols, C. I. O., and Mac, N. C. 2023. A Unified Intensity of the Magnetic Field in the Protoplanetary Disk from the Winchcombe Meteorite. *Meteoritics & Planetary Science* 59: 1194–1215. <https://doi.org/10.1111/maps.14079>.
- Bryson, J. F. J., Weiss, B. P., Biersteker, J. B., King, A. J., and Russell, S. S. 2020. Constraints on the Distances and Timescales of Solid Migration in the Early Solar System from Meteorite Magnetism. *The Astrophysical Journal* 896: 103.
- Bryson, J. F. J., Weiss, B. P., Lima, E. A., Gattacceca, J., and Cassata, W. S. 2020. Evidence for Asteroid Scattering and Distal Solar System Solids from Meteorite Paleomagnetism. *The Astrophysical Journal* 892: 126.
- Calvin, W. M., King, T. V. V., and Clark, R. N. 1994. Hydrous Carbonates on Mars? Evidence from Mariner 6/7 Infrared Spectrometer and Ground-Based Telescopic Spectra. *Journal of Geophysical Research* 99: 14659–75.
- Chennaoui Aoudjehane, H., Agee, C. B., Ziegler, K., Garvie, L. A. J., Irving, A., Sheikh, D., Carpenter, P. K., Zolensky, M., Schmitt-Kopplin, P., and Trif, L. 2021. Tarda, an Unusual Carbonaceous Chondrite Fall from Morocco. *84th Annual Meeting of the Meteoritical Society*, LPI Contribution No. 2609.
- Choe, W. H., Huber, H., Rubin, A. E., Kallemeyn, G. W., and Wasson, J. T. 2010. Compositions and Taxonomy of 15 Unusual Carbonaceous Chondrites. *Meteoritics & Planetary Science* 45: 531–554.
- Cody, G. D., and Alexander, C. M. O'D. 2005. NMR Studies of Chemical Structural Variation of Insoluble Organic Matter from Different Carbonaceous Chondrite Groups. *Geochimica et Cosmochimica Acta* 69: 1085–97.
- Cournède, C., Gattacceca, J., Gounelle, M., Rochette, P., Weiss, B., and Zanda, B. 2015. An Early Solar System Magnetic Field Recorded in CM Chondrites. *Earth and Planetary Science Letters* 410: 62–74.
- Cressey, G., and Schofield, P. F. 1996. Rapid Whole-Pattern Profile Stripping Method for the Quantification of Multiphase Samples. *Powder Diffraction* 11: 35–39.
- DeMeo, F. E., and Carry, B. 2014. Solar System Evolution from Compositional Mapping of the Asteroid Belt. *Nature* 505: 629–634.
- Donaldson Hanna, K. L., Thomas, I. R., Bowles, N. E., Greenhagen, B. T., Pieters, C. M., Mustard, J. F., Jackson, C. R. M., and Wyatt, M. B. 2012. Laboratory Emissivity Measurements of the Plagioclase Solid Solution Series under Varying Environmental Conditions. *Journal of Geophysical Research: Planets* 117: 1–7.
- Dotto, E., Fornasier, S., Barucci, M. A., Licandro, J., Boehnhardt, H., Hainaut, O., Marzari, F., de Bergh, C., and De Luise, F. 2006. The Surface Composition of Jupiter Trojans: Visible and near-Infrared Survey of Dynamical Families. *Icarus* 183: 420–434.
- Ehrenfreund, P., Robert, F., d'Hendecourt, L., and Behar, F. 1991. Comparison of Interstellar and Meteoritic Organic Matter at 3.4 μm . *Astronomy and Astrophysics* 252: 712–17.
- Endress, M., and Bischoff, A. 1996. Carbonates in CI chondrites: Clues to parent body evolution. *Geochimica et Cosmochimica Acta* 60: 489–507.
- Flynn, G. J., Keller, L. P., Feser, S., Wirick, S., and Jacobsen, C. 2003. The Origin of Organic Matter in the Solar System: Evidence from the Interplanetary Dust Particles. *Geochimica et Cosmochimica Acta* 67: 4791–4806.
- Fu, R. R., Weiss, B. P., Lime, E. A., Harrison, R. J., Bai, X.-N., Desch, S. J., Ebel, D. S., et al. 2014. Solar Nebula Magnetic Fields Recorded in the Semarkona Meteorite. *Science* 346: 1089–92.
- Fujiya, W., Hoppe, P., Ushikubo, T., Fukuda, K., Lindgren, P., Lee, M. R., Koike, M., Shirai, K., and Sano, Y. 2019. Migration of D-Type Asteroids from the Outer Solar System Inferred from Carbonate in Meteorites. *Nature Astronomy* 3: 910–15.
- Fujiya, W., Sugiura, N., Sano, Y., and Hiyagon, H. 2013. Mn-Cr Ages of Dolomite in CI Chondrites and the Tagish Lake Ungrouped Carbonaceous Chondrite. *Earth and Planetary Science Letters* 362: 130–142.
- Garenne, A., Beck, P., Montes-Hernandez, G., Chiriac, R., Toche, F., Quirico, E., Bonal, L., and Schmitt, B. 2014. The Abundance of Stability of “Water” in Type 1 and 2 Carbonaceous Chondrites (CI, CM and CR). *Geochimica et Cosmochimica Acta* 137: 93–112.

- Gattacceca, J., McCubbin, F. M., Grossman, J., Bouvier, A., Bullock, E., Chennaoui Aoudjehane, H., Debaille, V., et al. 2021. The Meteoritical Bulletin, No. 109. *Meteoritics & Planetary Science* 56: 1626–30.
- Ge, K., Williams, W., Nagy, L., and Tauxe, L. 2021. Models of Maghematization: Observational Evidence in Support of a Magnetic Unstable Zone. *Geochemistry, Geophysics, Geosystems* 22: e2020GC009504.
- Gilmour, C. M., Herd, C. D. K., and Beck, P. 2019. Water Abundance in the Tagish Lake Meteorite from TGA and IR Spectroscopy: Evaluation of Aqueous Alteration. *Meteoritics & Planetary Science* 54: 1951–72.
- Hamilton, V. E. 2010. Thermal Infrared (Vibrational) Spectroscopy of Mg-Fe Olivines: A Review and Applications to Determining the Compositions of Planetary Surfaces. *Chemie der Erde* 70: 7–33.
- Hamilton, V. E., Simon, A. A., Christensen, P. R., Reuter, D. C., Clark, B. E., Barucci, M. A., Bowles, N. E., et al. 2019. Evidence for Widespread Hydrated Minerals on Asteroid (101955) Bennu. *Nature Astronomy* 3: 332–340.
- Hanna, R. D., Hamilton, V. E., Haberle, C. W., King, A. J., Abreu, N. M., and Friedrich, J. M. 2020. Distinguishing Relative Aqueous Alteration and Heating among CM Chondrites with IR Spectroscopy. *Icarus* 346: 113760.
- Hewins, R. H., Zanetta, P.-M., Zanda, B., Le Guillou, C., Gattacceca, J., Sognzoni, C., Pont, S., et al. 2021. Northwest Africa (NWA) 12563 and Ungrouped C2 Chondrites: Alteration Styles and Relationships to Asteroids. *Geochimica et Cosmochimica Acta* 311: 238–273.
- Hiroi, T., Tonui, E., Pieters, C. M., Zolensky, M. E., Ueda, Y., Miyamoto, M., and Sasaki, S. 2005. Meteorite WIS 91600: A New Sample Related to a D- or T-Type Asteroid. *36th Lunar & Planetary Science Conference*, abstract #1564.
- Hiroi, T., Zolensky, M. E., and Pieters, C. M. 2001. The Tagish Lake Meteorite: A Possible Sample from a D-Type Asteroid. *Science* 293: 2234–36.
- Howard, K. T., Alexander, C. M. O'D., Schrader, D. L., and Dyl, K. A. 2015. Classification of Hydrous Meteorites (CR, CM and C2 Ungrouped) by Phyllosilicate Fraction: PSD-XRD Modal Mineralogy and Planetesimal Environments. *Geochimica et Cosmochimica Acta* 149: 206–222.
- Howard, K. T., Benedix, G. K., Bland, P. A., and Cressey, G. 2009. Modal Mineralogy of CM2 Chondrites by X-Ray Diffraction (PSD-XRD). Part 1: Total Phyllosilicate Abundance and the Degree of Aqueous Alteration. *Geochimica et Cosmochimica Acta* 73: 4576–89.
- Izawa, M. R. M., Craig, M. A., Applin, D. M., Sanchez, J. A., Reddy, V., Le Corre, L., Mann, P., and Cloutis, E. A. 2015. Variability, Absorption Features, and Parent Body Searches in “Spectrally Featureless” Meteorite Reflectance Spectra: Case Study—Tagish Lake. *Icarus* 254: 324–332.
- Jiang, Z., Liu, Q., Dekkers, M. J., Zhao, X., Roberts, A. P., Yang, Z., Jin, C., and Liu, J. 2017. Remagnetization Mechanisms in Triassic Red Beds from South China. *Earth and Planetary Science Letters* 479: 219–230.
- Kaplan, H. H., Lauretta, D. S., Simon, A. A., Hamilton, V. E., DellaGiustina, D. N., Golish, D. R., Reuter, D. C., et al. 2020. Bright Carbonate Veins on Asteroid (101955) Bennu: Implications for Aqueous Alteration History. *Science* 370: eabc3557.
- Kebukawa, Y., Alexander, C. M. O'D., and Cody, G. D. 2011. Compositional Diversity in Insoluble Organic Matter in Type 1, 2 and 3 Chondrites as Detected by Infrared Spectroscopy. *Geochimica et Cosmochimica Acta* 75: 3530–41.
- Kimura, Y., Sato, T., Nakamura, N., Nozawa, J., Nakamura, T., Tsukamoto, K., and Yamamoto, K. 2013. Vortex Magnetic Structure in Framboidal Magnetite Reveals Existence of Water Droplets in Ancient Asteroid. *Nature Communications* 4: 3649.
- King, A. J., Daly, L., Rowe, J., Joy, K. H., Greenwood, R. C., Devillepoix, H. A., Suttle, M. D., et al. 2022. The Winchcombe Meteorite, a Unique and Pristine Witness from the Outer Solar System. *Science Advances* 8: eabq3925.
- King, A. J., Schofield, P. F., Howard, K. T., and Russell, S. S. 2015. Modal Mineralogy of CI and CI-Like Chondrites by X-Ray Diffraction. *Geochimica et Cosmochimica Acta* 165: 148–160.
- King, A. J., Schofield, P. F., and Russell, S. S. 2021. Thermal Alteration of CM Carbonaceous Chondrites: Mineralogical Changes and Metamorphic Temperatures. *Geochimica et Cosmochimica Acta* 298: 167–190.
- King, A. J., Solomon, J. R., Schofield, P. F., and Russell, S. S. 2015. Characterising the CI and CI-Like Carbonaceous Chondrites Using Thermogravimetric Analysis and Infrared Spectroscopy. *Earth, Planets and Space* 67: 198.
- Lane, M. D., and Christensen, P. R. 1997. Thermal Infrared Emission Spectroscopy of Anhydrous Carbonates. *Journal of Geophysical Research: Planets* 102: 25581–92.
- Lauretta, D. S., Connolly, H. C., Jr., Aebersold, J. E., Alexander, C. M. O'D., Ballouz, R.-L., Barnes, J. J., Bates, H. C., et al. 2024. Asteroid (101955) Bennu in the Laboratory: Properties of the Sample Collected by OSIRIS-REx. *Meteoritics & Planetary Science*. <https://doi.org/10.1111/maps.14227>.
- Lee, M. R., Lindgren, P., and Sofo, M. R. 2014. Aragonite, Brunnerite, Calcite and Dolomite in the CM Carbonaceous Chondrites: High Fidelity Recorders of Progressive Parent Body Aqueous Alteration. *Geochimica et Cosmochimica Acta* 144: 126–156.
- Levison, H. F., Bottke, W. F., Gounelle, M., Morbidelli, A., Nesvorný, D., and Tsiganis, K. 2009. Contamination of the Asteroid Belt by Primordial Trans-Neptunian Objects. *Nature* 460: 364–66.
- Marrocchi, Y., Avicé, G., and Barrat, J.-A. 2021. The Tarda Meteorite: A Window into the Formation of D-Type Asteroids. *The Astrophysical Journal Letters* 913: L9.
- Maurel, C., and Gattacceca, J. 2023. Estimating Paleointensities from Chemical Remanent Magnetizations of Magnetite Using Non-heating Methods. *Journal of Geophysical Research: Planets* 128: e2023JE007779.
- Maurel, C., Gattacceca, J., and Uehara, M. 2024. Hayabusa2 Returned Samples Reveal a Weak to Null Magnetic Field During Aqueous Alteration of Ryugu's Parent Body. *Earth and Planetary Science Letters* 627: 118559.
- McClelland, E. 1996. Theory of CRM Acquired by Grain Growth, and its Implications for TRM Discrimination and Paleointensity Determination in Igneous Rocks. *Geophysical Journal International* 126: 271–280.
- Meerdink, S. K., Hook, S. J., Roberts, D. A., and Abbott, E. A. 2019. The ECOSTRESS Spectral Library Version 1.0. *Remote Sensing of Environment* 230: 111196.
- Morbidelli, A., Chambers, J., Lunine, J. I., Petit, J. M., Robert, F., Valsecchi, G. B., and Cyr, K. E. 2000. Source Regions and Timescales for the Delivery of Water to the Earth. *Meteoritics & Planetary Science* 35: 1309–20.

- Morbidelli, A., Levison, H. F., Tsiganis, K., and Gomes, R. 2005. Chaotic Capture of Jupiter's Trojan Asteroids in the Early Solar System. *Nature* 435: 462–65.
- Morin, G. L. F., Marrocchi, Y., Villeneuve, J., and Jacquet, E. 2022. 16O-Rich Anhydrous Silicates in CI Chondrites: Implications for the Nature and Dynamics of Dust in the Solar Accretion Disk. *Geochimica et Cosmochimica Acta* 332: 203–219.
- Nagy, L., Williams, W., Muxworthy, A. R., and Shcherbakov, V. P. 2017. Stability of Equidimensional Pseudo-Single-Domain Magnetite over Billion-Year Timescales. *Proceedings of the National Academy of Sciences of the United States of America* 114: 10356–60.
- Nakamura, T., Noguchi, T., Kimura, Y., Hiroi, T., Ahn, I., Lee, J. I., and Sasaki, S. 2013. MET00432: Another Tagish Lake-Type Carbonaceous Chondrite from Antarctica. *Meteoritics & Planetary Science* 48: 5122.
- Ono, H., Tsuchiyama, A., Matsumoto, M., Miyake, A., Matsuno, J., Nakamura, T., Yasutake, M., Uesugi, K., Takeuchi, A., and Tachibana, S. 2024. Development of 3D Crystal Shape Description Including Orientation Using NXCT and TEM and its Application to Ryugu Sample. *55th Lunar & Planetary Science Conference*, abstract #1488.
- Orthous-Daunay, F. R., Quirico, E., Beck, P., Brissaud, O., Dartois, E., Pino, T., and Schmitt, B. 2013. Mid-Infrared Study of the Molecular Structure Variability of Insoluble Organic Matter from Primitive Chondrites. *Icarus* 223: 534–543.
- Palmer, E. E., and Lauretta, D. S. 2011. Aqueous Alteration of Kamacite in CM Chondrites. *Meteoritics & Planetary Science* 46: 1587–1607.
- Quirico, E., Bonal, L., Beck, P., Alexander, C. M. O'D., Yabuta, H., Nakamura, T., Nakato, A., et al. 2018. Prevalence and Nature of Heating Processes in CM and C2-Ungrouped Chondrites as Revealed by Insoluble Organic Matter. *Geochimica et Cosmochimica Acta* 241: 17–37.
- Render, J., Bryson, J. F. J., Ebert, S., and Brennecke, G. A. 2022. Disk Transport Rates from Ti Isotopic Signatures of Refractory Inclusions. *Meteoritics & Planetary Science* 57: 2158–69.
- Rivkin, A. S., Volquardsen, E. L., and Clark, B. E. 2006. The Surface Composition of Ceres: Discovery of Carbonates and Iron-Rich Clays. *Icarus* 185: 563–67.
- Russell, S. S., Suttle, M. D., and King, A. J. 2022. Abundance and Importance of Petrological Type 1 Chondritic Material. *Meteoritics & Planetary Science* 57: 277–301.
- Salisbury, J. W., D'Aria, D. M., and Jarosewich, E. 1991. Midinfrared (2.5–23.5 μm) Reflectance Spectra of Powdered Stony Meteorites. *Icarus* 92: 280–297.
- Sato, M., Kimura, Y., Tanaka, S., Hatakeyama, T., Sugita, S., Nakamura, T., Tachibana, S., et al. 2022. Rock Magnetic Characterisation of Returned Samples from Asteroid (162173) Ryugu: Implications for Paleomagnetic Interpretation and Paleointensity Estimation. *Journal of Geophysical Research: Planets* 127: e2022JE007405.
- Schrader, D. L., Davidson, J., Foustoukos, D., Alexander, C. M. O'D., Torrano, Z. A., Cloutis, E. A., Applin, D. M., Zega, T. J., Nakamura, T., and Matsuoka, M. 2022. Tarda and Tagish Lake: Samples from the Same Outer Solar System Asteroid? *53rd Lunar & Planetary Science Conference*, abstract #1157.
- Simon, A. A., Kaplan, H. H., Hamilton, V. E., Lauretta, D. S., Campins, H. C., Emery, J. P., Barucci, M. A., et al. 2020. Widespread Carbon-Bearing Materials on near-Earth Asteroid (101955) Bennu. *Science* 370: eabc3522.
- Socrates, G. 2001. *Infrared and Raman Characteristic Group Frequencies: Tables and Charts*, 3rd ed. Chichester: John Wiley & Sons, Ltd.
- Sridhar, S., Bryson, J. F. J., King, A. J., and Harrison, R. J. 2021. Constraints on the Ice Composition of Carbonaceous Chondrites from their Magnetic Mineralogy. *Earth and Planetary Science Letters* 576: 117243.
- Suttle, M. D., King, A. J., Schofield, P. F., Bates, H., and Russell, S. S. 2021. The Aqueous Alteration of CM Chondrites, a Review. *Geochimica et Cosmochimica Acta* 299: 219–256.
- Takir, D., Emery, J. P., McSween, H. Y., Jr., Hibbitts, C. A., Clark, R. N., Pearson, N., and Wang, A. 2013. Nature and Degree of Aqueous Alteration in CM and CI Carbonaceous Chondrites. *Meteoritics & Planetary Science* 48: 1618–37.
- Tonui, E., Zolensky, M., Hiroi, T., Nakamura, T., Lipschutz, M. E., Wang, M.-S., and Okudaira, K. 2014. Petrographic, Chemical and Spectroscopic Evidence for Thermal Metamorphism in Carbonaceous Chondrites I: CI and CM Chondrites. *Geochimica et Cosmochimica Acta* 126: 284–306.
- Vacher, L. G., Piani, L., Rigaudier, T., Thomassin, D., Florin, G., Piralla, M., and Marrocchi, Y. 2020. Hydrogen in Chondrites: Influence of Parent Body Alteration and Atmospheric Contamination on Primordial Components. *Geochimica et Cosmochimica Acta* 281: 53–66.
- Vervelidou, F., Weiss, B. P., and Lagroix, F. 2023. Hand Magnets and the Destruction of Ancient Meteorite Magnetism. *Journal of Geophysical Research: Planets* 128: e2022JE007464.
- Weiss, B. P., Bai, X.-N., and Fu, R. R. 2021. History of the Solar Nebula from Meteorite Paleomagnetism. *Science Advances* 7: eaba5967.
- Weiss, B. P., and Tikoo, S. M. 2014. The Lunar Dynamo. *Science* 346: 1246753.
- Yabuta, H., Alexander, C. M. O'D., Fogel, M. L., Kilcoyne, A. L. D., and Cody, G. D. 2010. A Molecular and Isotopic Study of the Macromolecular Organic Matter of the Ungrouped C2 WIS 91600 and its Relationship to Tagish Lake and PCA 91008. *Meteoritics & Planetary Science* 45: 1446–60.
- Yamanobe, M., Nakamura, T., and Nakashima, D. 2018. Oxygen Isotope Reservoirs in the Outer Asteroid Belt Inferred from Oxygen Isotope Systematics of Chondrule Olivines and Isolated Forsterite and Olivine Grains in Tagish Lake-Type Carbonaceous Chondrites, WIS 91600 and MET 00432. *Polar Science* 15: 29–38.
- Yesiltas, M., and Kebukawa, Y. 2016. Associations of Organic Matter with Minerals in Tagish Lake Meteorite Via High Spatial Resolution Synchrotron-Based FTIR Microspectroscopy. *Meteoritics & Planetary Science* 51: 584–595.
- Yesiltas, M., Kebukawa, Y., Glotch, T. D., Zolensky, M., Fries, M., Aysal, N., and Tukul, F. S. 2022. Compositional and Spectroscopic Investigation of Three Ungrouped Carbonaceous Chondrites. *Meteoritics & Planetary Science* 57: 1665–87.
- Zolensky, M. E., Nakamura, K., Gounelle, M., Mikouchi, T., Kasama, T., Tachikawa, O., and Tonui, E. 2002. Mineralogy of Tagish Lake: An Ungrouped Type 2 Carbonaceous Chondrite. *Meteoritics & Planetary Science* 37: 737–761.

SUPPORTING INFORMATION

Additional supporting information may be found in the online version of this article.

Figure S1. Reflectance spectral maps of the polished Tarda samples were acquired using a spot size of $75 \times 75 \mu\text{m}$ and a step size (i.e., blue squares) of $75 \mu\text{m}$.

Figure S2. Areas of the polished Tarda samples with uneven surfaces appear brighter in the optical images. These areas were found to have CFs at longer wavelengths (top) and $3 \mu\text{m}$ features at shorter wavelengths (bottom) relative to the rest of the sample.

Figure S3. (a) The difference metric, D'_L , and (b) the uncertainty metric E_L , for all four specimens of Tarda calculated for coercivities greater than the MC component. The critical ranges of values are depicted by the grey bars.

Figure S4. ARM paleointensity determination for all four specimens of Tarda. The ARM had a $10 \mu\text{T}$ bias field. The fits (grey lines) and recovered paleointensities are included. The term '>MC' refers to the magnetisation at coercivities greater than the MC component.

Figure S5. Normalised NRM and ARMs lost for all four specimens of Tarda. The magnetisations are normalised to the values at the upper limit of the MC range (vertical, dashed grey lines) for each specimen. The NRMs are fully demagnetised (i.e., flat) to the right of these lines, while the ARMs all continue to lose magnetisation (i.e., not flat). The ARMs become flat at AF intensities $>75 \text{ mT}$.

Figure S6. Tarda contains distinct, porous clasts whose spectra show deep $3.4 \mu\text{m}$ features (top left and right) and complex reflectance minima near $6 \mu\text{m}$ (bottom left and right) that are not observed elsewhere on the sample.

Figure S7. Example mid-IR spectra acquired from polished samples of Tarda using micro-IR spectroscopy. Spectral features in this region are attributed to a combination of phyllosilicates, anhydrous silicates, and carbonates.

Table S1. Bulk modal mineralogy of Tarda and Tagish Lake measured using position-sensitive-detector X-ray diffraction. Data for Tagish Lake are from Bland et al. (2004).

Table S2. TGA mass loss as a function of temperature for Tarda (this study and Yesiltas et al., 2022), the CI chondrite Orgueil, Tagish Lake, and the CM chondrite Murchison. Data for Orgueil are from King et al. (2015). Data for Tagish Lake and Murchison are the average of five aliquots analysed by Gilmour et al. (2019) and King et al. (2021), respectively.

Table S3. AF demonisation parameter for the four specimens of Tarda. Because there is no resolvable component at coercivities greater than the MC component, we refer to this coercivity range as >MC rather than a high coercivity component.

Table S4. Paleointensities and 95% uncertainties recovered from all four specimens of Tarda.